Hindawi
International Journal of Intelligent Systems
Volume 2023, Article ID 7626478, 32 pages
https://doi.org/10.1155/2023/7626478

Research Article

Neuro-Heuristic Computational Intelligence Approach for Optimization of Electro-Magneto-Hydrodynamic Influence on a Nano Viscous Fluid Flow

Zeeshan Ikram Butt,[1] **Iftikhar Ahmad**,[1] **Muhammad Asif Zahoor Raja**,[2] **Syed Ibrar Hussain**,[3] **Muhammad Shoaib**,[4] **and Hira Ilyas**[5]

[1]*Department of Mathematics, University of Gujrat, Gujrat 50700, Pakistan*
[2]*Future Technology Research Centre, National Yunlin University of Science and Technology, 123 University Road, Section 3, Douliou, Yunlin 64002, Taiwan*
[3]*Dipartimento di Matematica e Informatica, Università degli Studi di Palermo, Via Archirafi 34, Palermo 90123, Italy*
[4]*Yuan Ze University, AI Center, Taoyuan 320, Taiwan*
[5]*Department of Physical Sciences, University of Chenab, Gujrat 50700, Pakistan*

Correspondence should be addressed to Syed Ibrar Hussain; syedibrar.hussain@unipa.it

Received 12 June 2023; Revised 19 November 2023; Accepted 27 November 2023; Published 16 December 2023

Academic Editor: Mohammad R. Khosravi

In this investigative study, the electro-magneto hydrodynamic (EMHD) influence on a nano viscous fluid model is scrutinized by designing an artificial neural network (ANN) paradigm using a neuro-heuristic approach (NHA) through the combination of GAs (genetic algorithms) and one of the most efficient locally searching solver SQP (sequential quadratic programming), i.e., NHA-GA-SQP. The fluid flow for the proposed problem is initially interpreted in the form of PDEs and then utilization of suitable similarity transformation on these PDEs yields in terms of a stiff nonlinear system of ODEs. The numerical results of the suggested fluidic model based on the variation of its physically existing parameters are calculated through the NHA-GA-SQP solver to detect the variation in velocity, thermal gradient, and concentration during the fluid flow. A detailed analysis of obtained outcomes through the NHA-GA-SQP algorithm and their comparison with the reference results estimated via the Adams method are presented. The calculation of the proposed solver's accuracy, stability, and consistency through various statistical operators is also involved in the current inspection.

1. Introduction

Nanofluids (NFs) have been proving an effective source of heat transfer for the last two decades. The base liquids such as oil, water, ethylene glycol, and alcohol (liquor) are not capable of enhancing the thermal rate, and to overcome this flaw, nanometer-sized tiny particles were mixed with base fluids to produce NFs [1]. These nanometer-sized tiny particles are defined as nanoparticles and are found in shapes such as nitrides, carbides, oxides, and metals [2–4]. Choi and Eastman [5] was the pioneer of nanoparticles who claimed that the mixing of nanoparticles with base fluids can considerably enhance their thermal characteristics. Ramesh et al. [6] and Nguyen and Ahn [7] scrutinized that NFs are known as heat transfer fluids using nanoparticles. Heat transfer is an important application of engineering for units such as engines, nuclear reactors, and power plants. Major uses of heat transfer at the industrial level are biomedical, petroleum, electronics, automotive, and food [8]. Because of their effective ability of heat transfer, NFs have been utilized in car radiators [9], cooling systems [10], solar energy devices [11], and electric battery cooling [12]. Nadeem et al. [13] examined bio-convection forced flow in a viscous NF. They also discussed the heat with mass transmission (HMT)

in carbon nanotubes [14, 15]. Alzahrani et al. [16] studied HMT in Casson nanoliquid along a stretchy surface. Khan et al. [17] explored the viscous NF model using three nanoparticles. Ahmad et al. [18, 19] investigated HMT using various nanoliquid paradigms. EMHD is defined as the coupling of a fluid flow and electric current in the presence of an electromagnetic field and has a strong effect on the behavior of NFs. The NFs' overall heat transfer properties are changed when electromagnetic fields align nanoparticles to improve thermal conductivity. MHD effects affect the fluid flow patterns, pressure, and velocity when electrically conductive nanofluids interact with electromagnetic fields. NF's rheological behavior is also impacted by EMHD, which modifies their viscosity. The distribution of nanoparticles in a fluid is regulated, and agglomeration is prevented by dielectrophoretic forces, which are produced by irregular electric fields. EMHD effects in NFs are involved in various fields like plasma studies, magnetic insulation of cells, optics, drug delivery, optical controlling of switches, biomedicine, blood flow measurement, etc. Reddy et al. [20] numerically examined hybrid form NF with EMHD effects using the bvp4c technique and observed an uplift in temperature profile by enhancing thermal radiation. Obalalu et al. [21] studied the heat transfer phenomenon through an implication of EMHD along a stretched surface on NF using the Chebyshev wavelets technique. Saha et al. [22] investigated Jeffery NF with stratified boundary conditions under the impact of EMHD using the optimal homotopy analysis method and observed a rise in NF temperature by uplifting the thermal radiation parameter. Naz et al. [23] examined entropy generation in NFs along with the MHD effect. Tlili et al. [24] discussed the MHD effect in hybrid NFs. Al-Farhany et al. [25] scrutinized the MHD effect in ferrofluid. Zaman and Gul [26] examined the MHD effect in Williamson NF. Ayub et al. [27] scrutinized the heat transfer phenomenon by applying the shooting method on steady-state micropolar fluid. Some useful research related to DEs by numerical techniques is presented by Ahmad et al. in [28–32].

ANNs are established to examine mathematical systems in the shape of a computational frame of work. It is a brain-inspired system that completely works on neurons. Recently, ANN-based numerical techniques have been extensively employed to solve real-world problems in various fields like medicine, biomedical, engineering, finance, geology, welding, and material science. Many academics have adopted ANN-based computational solvers including supervised and unsupervised learning to obtain approximate numerical solutions in different sectors of applied sciences like food recognition [33], cyberattack detection in interconnected power control systems, speech emotion recognition, COVID-19 [34], AVR system robust design [35], organ segmentation and dose prediction [36], voice mood recognition [37], slung-load system control in helicopters [38], robust motor control model [39], food freshness prediction [40], water and fat separation model [41], lung functional MRI [42], FRAPPE model [43], kidney disease model [44], corneal shape paradigm [45], Emden-Fowler model, wind power, SITR model, and Thomas-Fermi model [46–49]. Some important works based on ANNs are presented in [50–52]. Indeed, the abovementioned list of literature is an indication of the purposeful use of ANNs on a large scale, but the dynamics of the EMHD effect on a viscous nanofluid model using the NHA-GA-SQP algorithm are yet to be explored. A list of innovative contributions of the current study is listed as follows:

(i) A new NHA-GA-SQP technique is developed and applied to get the best approximate solution of the nonlinear ODEs system transformed through PDEs of the suggested nanofluidic model

(ii) The dynamics of the nano viscous fluid model are studied in detail using different scenarios based on alteration in the numerical values of various involved physical parameters to scrutinize the velocity profile, thermal gradient, and nanoparticle concentration of the suggested problem

(iii) The accuracy of NHA-GA-SQP technique is evaluated in each scenario through well-known statistical operators

(iv) The convergence rate of the proposed solver is verified through fitness estimation for all scenarios

2. Mathematical Modeling

The laminar fluid flow of mixed convective type with nanoparticles under MHD impact past a stretchy face surface is explored. The stretchy surface is examined here in the Cartesian coordinate system. Thermophoresis along with Brownian motion effects is also included in the suggested fluid model. Moreover, Joule heating, heat source/sink, and viscous dissipation are also involved in the flow. Figure 1 demonstrates the geometry of flow for the proposed model.

Physical behavior based on irreversibility in viscous laminar nanomaterials flow along with chemical reaction is also examined in the presence of both magnetic and electric fields in the region $y > 0$. Both the fields are originated from Ohm's law $\mathbf{J} = \sigma(\mathbf{E} + \mathbf{V} \times \mathbf{B})$ in which $\mathbf{J}$ represents the amount of Joule current, while σ expresses electrical conductivity. If b represents the stretching parameter then v_{1w} represents the velocity of stretching sheet.

The governing system of the recommended model integrated through the irreversibility phenomena is given as follows:

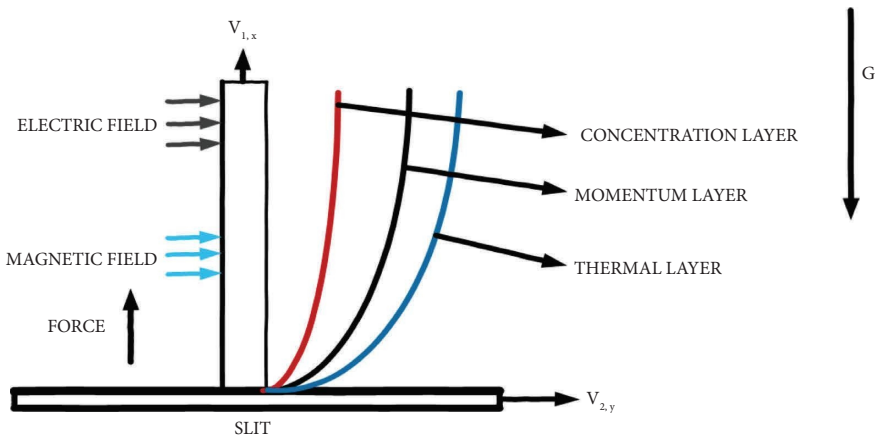

Figure 1: Schematic structure of the nano viscous fluid model.

$$\frac{\partial v_1}{\partial x}+\frac{\partial v_2}{\partial y}=0,$$

$$v_2\frac{\partial v_1}{\partial y}+v_1\frac{\partial v_1}{\partial x}=-\frac{1}{\rho_g}\frac{\partial p}{\partial x}+\frac{\partial^2 v_1}{\partial y^2}\nu+\left(EB-B^2v_1\right)\frac{\sigma}{\rho_g}+\beta_c\left(C-C_\infty\right)+\frac{G}{\rho_g}\left(\beta_t\left(\mathrm{Tm}-\mathrm{Tm}_\infty\right)\right),$$

$$v_1\frac{\partial \mathrm{Tm}}{\partial x}+v_2\frac{\partial \mathrm{Tm}}{\partial y}=\frac{\mu}{\left(\rho c_p\right)_g}\left(\frac{\partial v_1}{\partial y}\right)^2+\alpha\frac{\partial^2 \mathrm{Tm}}{\partial y^2}+\left(D_B\frac{\partial C}{\partial y}\frac{\partial \mathrm{Tm}}{\partial y}+\frac{D_T}{Tm_\infty}\left(\frac{\partial \mathrm{Tm}}{\partial y}\right)^2\right)\tau+\frac{Q_0}{\left(\rho c_p\right)_g}\left(\mathrm{Tm}-\mathrm{Tm}_\infty\right)+\frac{\sigma}{\left(\rho c_p\right)_g}\left(v_1B-EB\right)^2, \quad (1)$$

$$v_1\frac{\partial C}{\partial x}+v_2\frac{\partial C}{\partial y}=\frac{\partial^2 C}{\partial y^2}D_B-k_1\left(\left(C-C_\infty\right)\right)+\frac{\partial^2 \mathrm{Tm}}{\partial y^2}\frac{D_T}{\mathrm{Tm}_\infty},$$

$$\left.\begin{aligned} &v_1=v_{1w}(x)=\mathrm{bx}, \quad \mathrm{Tm}=\mathrm{Tm}_w, \quad v_2=0, \quad C=C_w \text{ at } y=0\\ &v_1=0, \quad v_2=0, \quad C\longrightarrow C_\infty, \quad \mathrm{Tm}\longrightarrow \mathrm{Tm}_\infty \text{ when } y\longrightarrow\infty \end{aligned}\right\}.$$

Applying the transformations,

We get

$$\left.\begin{aligned} &v_1=\mathrm{xbg}'(\xi), \quad v_2=-g(\xi)\sqrt{\mathrm{b}\nu_2}\\ &\phi(\xi)=\frac{C-C_\infty}{C_w-C_\infty}, \quad \theta(\xi)=\frac{\mathrm{Tm}-\mathrm{Tm}_\infty}{\mathrm{Tm}_w-\mathrm{Tm}_\infty}, \quad \xi=y\sqrt{\frac{b}{\nu_2}} \end{aligned}\right\}. \quad (2)$$

$$g'''+g''g-g'^2+\left(E_1-g'\right)M+\left(N_1\phi+\theta\right)\lambda=0,$$

$$\theta''+\mathrm{Pr}\,\theta' g+\left(\mathrm{Nt}\,\theta'^2+\mathrm{Nb}\,\theta'\phi'\right)\mathrm{Pr}+M\left(g'-E_1\right)^2\mathrm{Br}+\beta\theta \quad \mathrm{Pr}=0,$$

$$\phi''+\theta''\frac{\mathrm{Nt}}{\mathrm{Nb}}+\mathrm{Sc}\,g\,\phi'-\gamma\,\phi\,\mathrm{Sc}=0, \quad (3)$$

$$\left.\begin{aligned} &g(0)=0, \quad g'(0)=1, \quad \phi(0)=1, \quad \theta(0)=1\\ &\theta(\infty)=0, \quad g'(\infty)=0, \quad \phi(\infty)=0 \end{aligned}\right\}.$$

Here, $M = (\sigma B_0^2/b\rho_g)$ represents the magnetic parameter, $E_1 = (E_0/B_0 v_{1w})$ denotes the electric field parameter, $\lambda = (\mathrm{Gr}/\mathrm{Re}^2)$ is called the mixed convection parameter, $\mathrm{Gr} = (G\beta_t(\mathrm{Tm}_w - \mathrm{Tm}_\infty)x^3/\rho_g {\nu_2}^2)$ represents the Grashof number, $\mathrm{Re} = (v_{1w}x/\upsilon)$ represents the local Reynolds number, $N_1 = (\beta_c(C_w - C_\infty)/\beta_t(\mathrm{Tm}_w - \mathrm{Tm}_\infty))$ is called the buoyancy ratio parameter, $\mathrm{Pr} = (\nu_2/\alpha)$ represents the Prandtl number, $\mathrm{Nt} = (\tau D_T(\mathrm{Tm}_w - \mathrm{Tm}_\infty)/\mathrm{Tm}_\infty \upsilon)$ is the thermophoresis parameter, $\mathrm{Ec} = ((\mathrm{bx})^2/c_p(\mathrm{Tm}_w - \mathrm{Tm}_\infty))$ denotes the Eckert number, $\mathrm{Nb} = (\tau D_B(C_w - C_\infty)/\upsilon)$ is called the Brownian motion parameter, $\mathrm{Br} = \mathrm{Pr}.\mathrm{Ec}$ denotes the Brinkman number, $\beta = Q_0/b(\rho c_p)_g$ is called the heat generation/absorption parameter, $\mathrm{Sc} = (\upsilon/D_B)$ represents the Schmidt number, and $\gamma = (k_1/b)$ is called the reaction parameter.

3. Proposed Methodology

In the current research, the form of approximate solution and its j^{th} order derivatives are

$$[\widehat{g}(\eta), \widehat{\theta}(\eta), \widehat{\phi}(\eta)] = \left[\sum_{q=1}^{n} \alpha_{1g,q} F\left(\alpha_{2g,q}\eta + \alpha_{3g,q}\right), \sum_{q=1}^{n} \alpha_{1\theta,q} F\left(\alpha_{2\theta,q}\eta + \alpha_{3\theta,q}\right), \sum_{q=1}^{n} \alpha_{1\phi,q} F\left(\alpha_{2\phi,q}\eta + \alpha_{3\phi,q}\right)\right], \tag{4}$$

$$\left[\widehat{g^{(j)}}(\eta), \widehat{\theta^{(j)}}(\eta), \widehat{\phi^{(j)}}(\eta)\right] = \left[\sum_{q=1}^{n} \alpha_{1g,q} F^{(j)}\left(\alpha_{2g,q}\eta + \alpha_{3g,q}\right), \sum_{q=1}^{n} \alpha_{1\theta,q} F^{(j)}\left(\alpha_{2\theta,q}\eta + \alpha_{3\theta,q}\right), \sum_{q=1}^{n} a*_{\phi,q} F^{(j)}\left(\alpha_{2\phi,q}\eta + \alpha_{3\phi,q}\right)\right], \tag{5}$$

α_1, α_2, and α_3 represent the unknown weights, and in vector form, they can be expressed as

$$s - t \quad \begin{aligned} W &= [W_g, W_\theta, W_\phi], \\ W_g &= [\alpha_{1g}, \alpha_{2g}, \alpha_{3g}], \\ W_\theta &= [\alpha_{1\theta}, \alpha_{2\theta}, \alpha_{3\theta}], \\ W_\phi &= [\alpha_{1\phi}, \alpha_{2\phi}, \alpha_{3\phi}]. \end{aligned} \tag{6}$$

In the aforementioned vectors, the components used are

$$\begin{aligned} \alpha_{1g} &= [\alpha_{1g,1}, \alpha_{1g,2}, \cdots, \alpha_{1g,n}], \\ \alpha_{1\theta} &= [\alpha_{1\theta,1}, \alpha_{1\theta,2}, \cdots, \alpha_{1\theta,n}], \\ \alpha_{1\phi} &= [\alpha_{1\phi,1}, \alpha_{1\phi,2}, \cdots, \alpha_{1\phi,n}], \\ \alpha_{2g} &= [\alpha_{2g,1}, \alpha_{2g,2}, \cdots, \alpha_{2g,n}], \\ \alpha_{2\theta} &= [\alpha_{2\theta,1}, \alpha_{2\theta,2}, \cdots, \alpha_{2\theta,n}], \\ \alpha_{2\phi} &= [\alpha_{2\phi,1}, \alpha_{2\phi,2}, \cdots, \alpha_{2\phi,n}], \\ \alpha_{3g} &= [\alpha_{3g,1}, \alpha_{3g,2}, \cdots, \alpha_{3g,n}], \\ \alpha_{3\theta} &= [\alpha_{3\theta,1}, \alpha_{3\theta,2}, \cdots, \alpha_{3\theta,n}], \\ \alpha_{3\phi} &= [\alpha_{3\phi,1}, \alpha_{3\phi,2}, \cdots, \alpha_{3\phi,n}], \end{aligned} \tag{7}$$

The function $F(\eta) = (1/(1 + e^{-\eta}))$ is known as log-sigmoid-based activation function in the current research having tendency to transfer input values to a range between 0 and 1. It offers smooth transitions between the extremes. The log sigmoid activation function facilitates the representation of complex interactions in the microviscous flow optimization situation within the context of our neuro heuristic computational intelligence methodology. The log sigmoid function enhances the overall performance of our optimization framework by providing nonlinearity and differentiability, which facilitate the neural network's ability to recognize intricate patterns and subtleties in the data. After substituting the value of activation function in the assumed approximate solution, the obtained equations are

$$[\widehat{g}(\eta), \widehat{\theta}(\eta), \widehat{\phi}(\eta)] = \left[\sum_{q=1}^{n} \frac{\alpha_{1g,q}}{1 + e^{-\left(\alpha_{2g,q}\eta + \alpha_{3g,q}\right)}}, \sum_{q=1}^{n} \frac{\alpha_{1\theta,q}}{1 + e^{-\left(\alpha_{2\theta,q}\eta + \alpha_{3\theta,q}\right)}}, \sum_{q=1}^{n} \frac{\alpha_{1\phi,q}}{1 + e^{-\left(\alpha_{2\phi,q}\eta + \alpha_{3\phi,q}\right)}}\right],$$

$$\widehat{g'''}(\eta) = \sum_{q=1}^{n}\left[\alpha_{1g,q}\alpha_{2g,q}^{3}\left(\frac{6e^{-3\left(\alpha_{2g,q}\eta + \alpha_{3g,q}\right)}}{\left(1 + e^{-\left(\alpha_{2g,q}\eta + \alpha_{3g,q}\right)}\right)^4} - \frac{6e^{-2\left(\alpha_{2g,q}\eta + \alpha_{3g,q}\right)}}{\left(1 + e^{-\left(\alpha_{2g,q}\eta + \alpha_{3g,q}\right)}\right)^3} + \frac{e^{-\left(\alpha_{2g,q}\eta + \alpha_{3g,q}\right)}}{\left(1 + e^{-\left(\alpha_{2g,q}\eta + \alpha_{3g,q}\right)}\right)^2}\right)\right],$$

$$\widehat{\theta''}(\eta) = \sum_{q=1}^{n}\left[\alpha_{1\theta,q}\alpha_{2_{\theta,q}}{}^{2}\left(\frac{2e^{-2\left(\alpha_{2\theta,q}\eta+\alpha_{3\theta,q}\right)}}{\left(1+e^{-\left(\alpha_{2\theta,q}\eta+\alpha_{3\theta,q}\right)}\right)^{3}} - \frac{e^{-\left(\alpha_{2\theta,q}\eta+\alpha_{3\theta,q}\right)}}{\left(1+e^{-\left(\alpha_{2\theta,q}\eta+\alpha_{3\theta,q}\right)}\right)^{2}}\right)\right],$$

$$\widehat{\phi''}(\eta) = \sum_{q=1}^{n}\left[\alpha_{1\phi,q}\alpha_{2\phi,q}^{2}\left(\frac{2e^{-2\left(\alpha_{2\phi,q}\eta+\alpha_{3\phi,q}\right)}}{\left(1+e^{-\left(\alpha_{2\phi,q}\eta+\alpha_{3\phi,q}\right)}\right)^{3}} - \frac{e^{-\left(\alpha_{2g,q}\eta+\alpha_{3g,q}\right)}}{\left(1+e^{-\left(\alpha_{2g,q}\eta+\alpha_{3g,q}\right)}\right)^{2}}\right)\right]'. \tag{8}$$

Formulation of suitable fitness function is

$$e_1 = \frac{1}{N}\sum_{k=1}^{N}\left(g_k''' + g_k'' g_k - g_k'^{2} + (E_1 - g_k')M + (N_1\phi_l + \theta_k)\lambda\right)^{2}, \tag{9}$$

$$e_1 * = \frac{1}{N}\sum_{k=1}^{N}\left(\theta_k'' + \mathrm{Pr}\theta_k' g_k + \left(\mathrm{Nt}\,\theta_k'^{2} + \mathrm{Nb}\,\theta_k'\phi_k'\right)\mathrm{Pr} + M\left(g_k' - E_1\right)^{2}\mathrm{Br} + \beta\,\theta_k\mathrm{Pr}\right)^{2}, \tag{10}$$

$$e_1 ** = \frac{1}{N}\sum_{k=1}^{N}\left(\phi_k'' + \theta_k''\frac{\mathrm{Nt}}{\mathrm{Nb}} + \mathrm{Sc}\,g_k\phi_k' - \gamma\,\phi_k\,\mathrm{Sc}\right)^{2}, \tag{11}$$

$$e_1 *** = \frac{1}{9}\left[g_1{}^{2} + \left(g_1{}' - 1\right)^{2} + \left(\theta_1 - 1\right)^{2} + \left(\phi_1 - 1\right)^{2} + g_N{}'^{2} + \theta_N{}^{2} + \phi_N{}^{2}\right], \tag{12}$$

$$E = \left[e_1 + e_1 * + e_1 ** + e_1 ***\right]. \tag{13}$$

Here, $N = (1/h)$, $\widehat{g}_k = \widehat{g}(\eta_k)$ and $\eta_k = \mathrm{kh}$. Equations (9)–(13) represent the value of error functions, and equation (12) is the representation of boundary conditions of the current problem.

3.1. Optimization of Networks. GAs' technique design is likewise natural growth structure, and this technique was introduced in 1960 by Holland [53]. GAs depict optimized performances of heuristic, selection, and mutation along with crossover and have many implementations including the aircrafts industry [54], solar photovoltaic systems [55], heterogeneous celebrations [56], weather forecasting [57], and pharmaceutical supply chain [58]. A hybridization of GAs with any local solver can significantly increase the convergence, and for this purpose, SQP solver is used [59, 60]. SQP most recent applications are charging of batteries, dairy field, hybrid electric vehicles [61], and virotherapy of cancer [62]. Figure 2 graphically depicts the optimization procedure of the NHA-GA-SQP algorithm used, while Algorithm 1 provides the details of the pseudocode constructed through NHA-GA-SQP.

3.2. Performance Matrix. To investigate the performance of the NHA-GA-SQP algorithm, the following statistical operators are used:

(i) E-VAF (*variance-account-for*)

(ii) RMSE (*root-mean-square error*)

(iii) E-NSE (*Nash–Sutcliffe efficiency*)

(iv) E-R^2 (*error function based on the coefficient of determination*)

(v) E-TIC (*Theil's coefficient for in-equality*)

With mathematical formulation,

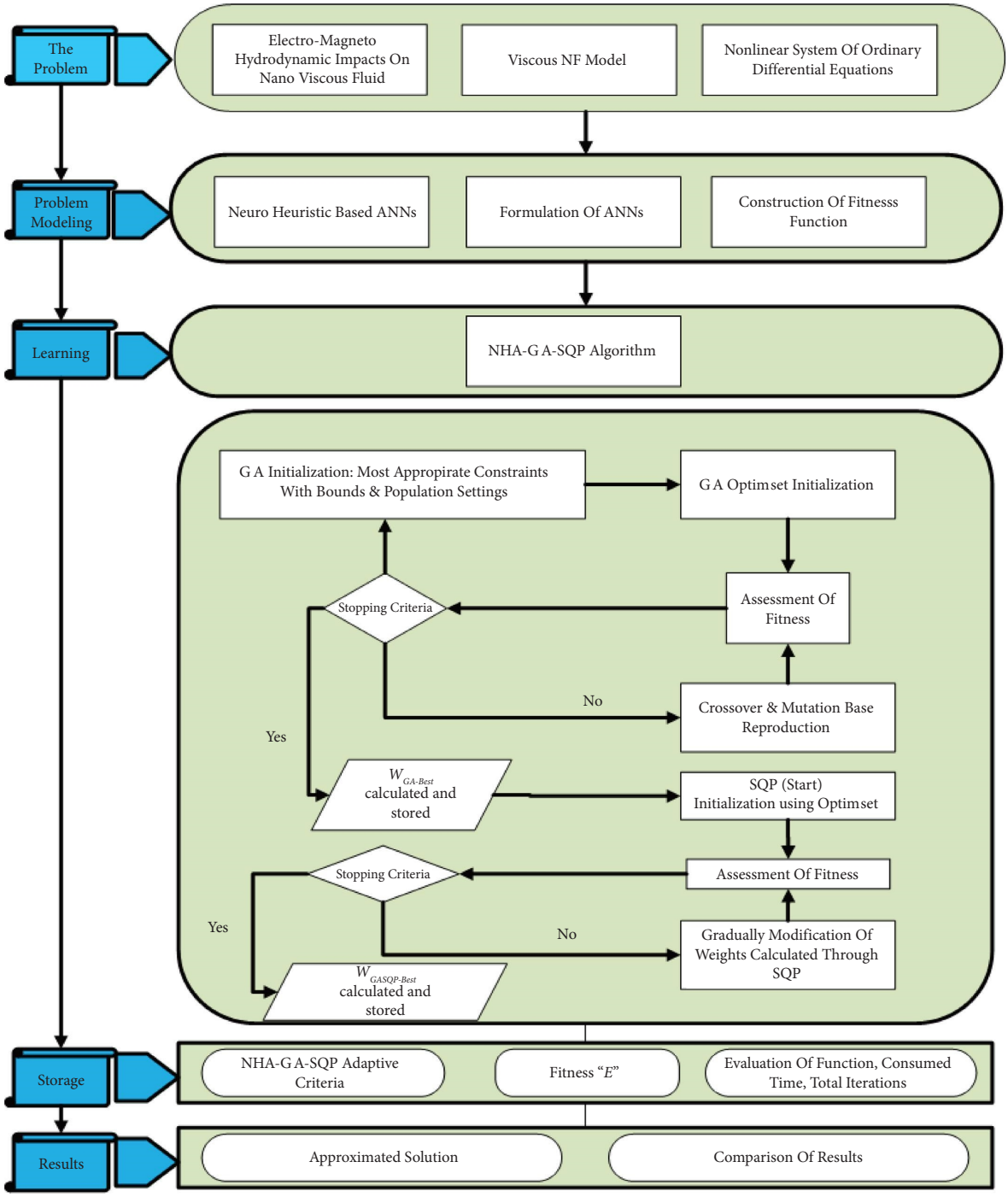

Figure 2: NHA-GA-SQP based graphical abstract for solving the current nanofluidic model.

$$\begin{bmatrix} \mathrm{RMSE}_{\widehat{g}} \\ \mathrm{RMSE}_{\widehat{\theta}} \\ \mathrm{RMSE}_{\widehat{\phi}} \end{bmatrix}_{\mathrm{NVF}} = \begin{bmatrix} \sqrt{\frac{1}{n}\sum_{q=1}^{n}\left(\widehat{g}_q - g_{\mathrm{ref}:q}\right)^2} \\ \sqrt{\frac{1}{n}\sum_{q=1}^{n}\left(\widehat{\theta}_q - \theta_{\mathrm{ref}:q}\right)^2} \\ \sqrt{\frac{1}{n}\sum_{q=1}^{n}\left(\widehat{\phi}_q - \phi_{\mathrm{ref}:q}\right)^2} \end{bmatrix}_{\mathrm{NVF}},$$

$$\begin{bmatrix} R^2_{\widehat{g}} \\ R^2_{\widehat{\theta}} \\ R^2_{\widehat{\phi}} \end{bmatrix}_{\mathrm{NVF}} = \begin{bmatrix} \frac{SS_{\mathrm{reg}:g}}{SS_{\mathrm{total}:g}} \\ \frac{SS_{\mathrm{reg}:\theta}}{SS_{\mathrm{total}:\theta}} \\ \frac{SS_{\mathrm{reg}:\phi}}{SS_{\mathrm{total}:\theta}} \end{bmatrix}_{\mathrm{NVF}},$$

$$\begin{bmatrix} \mathrm{NSE}_{\widehat{g}} \\ \mathrm{NSE}_{\widehat{\theta}} \\ \mathrm{NSE}_{\widehat{\phi}} \end{bmatrix}_{\mathrm{NVF}} = \begin{bmatrix} 1 - \frac{\sum_{q=1}^{n}\left(\widehat{g}_q - g_{\mathrm{ref}:q}\right)^2}{\sum_{q=1}^{n}\left(\widehat{g}_q - \overline{g_q}\right)^2} \\ 1 - \frac{\sum_{q=1}^{n}\left(\widehat{\theta}_q - \theta_{\mathrm{ref}:q}\right)^2}{\sum_{q=1}^{n}\left(\widehat{\theta}_q - \overline{\theta_q}\right)^2} \\ 1 - \frac{\sum_{q=1}^{n}\left(\widehat{\phi}_q - \phi_{\mathrm{ref}:q}\right)^2}{\sum_{q=1}^{n}\left(\widehat{\phi}_q - \overline{\phi_q}\right)^2} \end{bmatrix}_{\mathrm{NVF}},$$

$$\begin{bmatrix} \mathrm{VAF}_{\widehat{g}} \\ \mathrm{VAF}_{\widehat{\theta}} \\ \mathrm{VAF}_{\widehat{\phi}} \end{bmatrix}_{\mathrm{NVF}} = \begin{bmatrix} \left(1 - \frac{\mathrm{var}\left(g_{\mathrm{ref}:q} - \widehat{g}_q\right)}{\mathrm{var}\left(g_q\right)}\right) \times 100 \\ \left(1 - \frac{\mathrm{var}\left(\theta_{\mathrm{ref}:q} - \widehat{\theta}_q\right)}{\mathrm{var}\left(\theta_q\right)}\right) \times 100 \\ \left(1 - \frac{\mathrm{var}\left(\phi_{\mathrm{ref}:q} - \widehat{\phi}_q\right)}{\mathrm{var}\left(\phi_q\right)}\right) \times 100 \end{bmatrix}_{\mathrm{NVF}},$$

$$\begin{bmatrix} \mathrm{TIC}_{\widehat{g}} \\ \mathrm{TIC}_{\widehat{\theta}} \\ \mathrm{TIC}_{\widehat{\phi}} \end{bmatrix}_{\mathrm{NVF}} = \begin{bmatrix} \frac{\sqrt{(1/n)\sum_{q=1}^{n}\left(\widehat{g}_q - g_{\mathrm{ref}:q}\right)^2}}{\sqrt{(1/n)\sum_{q=1}^{n}\widehat{g}_q^{\,2}} + \sqrt{(1/n)\sum_{q=1}^{n}g^2_{\mathrm{ref}:q}}} \\ \frac{\sqrt{(1/n)\sum_{q=1}^{n}\left(\widehat{\theta}_q - \theta_{\mathrm{ref}:q}\right)^2}}{\sqrt{(1/n)\sum_{q=1}^{n}\widehat{\theta}_q^{\,2}} + \sqrt{(1/n)\sum_{q=1}^{n}\theta^2_{\mathrm{ref}:q}}} \\ \frac{\sqrt{(1/n)\sum_{q=1}^{n}\left(\widehat{\phi}_q - \phi_{\mathrm{ref}:q}\right)^2}}{\sqrt{(1/n)\sum_{q=1}^{n}\widehat{\phi}_q^{\,2}} + \sqrt{(1/n)\sum_{q=1}^{n}\phi^2_{\mathrm{ref}:q}}} \end{bmatrix}_{\mathrm{NVF}},$$

$$\begin{bmatrix} E - \mathrm{VAF}_{\widehat{g}} \\ E - \mathrm{VAF}_{\widehat{\theta}} \\ E - \mathrm{VAF}_{\widehat{\phi}} \end{bmatrix}_{\mathrm{NVF}} = \begin{bmatrix} 100 - \mathrm{VAF}_{\widehat{g}} \\ 100 - \mathrm{VAF}_{\widehat{\theta}} \\ 100 - \mathrm{VAF}_{\widehat{\phi}} \end{bmatrix}_{\mathrm{NVF}},$$

$$\begin{bmatrix} E - R^2_{\widehat{g}} \\ E - R^2_{\widehat{\theta}} \\ E - R^2_{\widehat{\phi}} \end{bmatrix}_{\mathrm{NVF}} = \begin{bmatrix} 1 - R^2_{\widehat{g}} \\ 1 - R^2_{\widehat{\theta}} \\ 1 - R^2_{\widehat{\phi}} \end{bmatrix}_{\mathrm{NVF}},$$

$$\begin{bmatrix} E - \mathrm{NSE}_{\widehat{g}} \\ E - \mathrm{NSE}_{\widehat{\theta}} \\ E - \mathrm{NSE}_{\widehat{\phi}} \end{bmatrix}_{\mathrm{NVF}} = \begin{bmatrix} 1 - \mathrm{NSE}_{\widehat{g}} \\ 1 - \mathrm{NSE}_{\widehat{\theta}} \\ 1 - \mathrm{NSE}_{\widehat{\phi}} \end{bmatrix}_{\mathrm{NVF}}. \tag{14}$$

4. Results and Discussion

A new algorithm NHA-GA-SQP is used to solve the nano viscous fluid flow problem numerically by applying an appropriate optim setting, and the best calculated trained weights involved in searching the best numerical outcomes of the suggested problem are illustrated through Figures 3–9 based on seven different scenarios whose details are provided in Table 1. The implementation of these trained weights in equation (4) provides the solution to the proposed problem. To measure the suitability of the hybridization used in the NHA-GA-SQP algorithm for fast convergence, learning curves obtained for one case of the 1st scenario are also portrayed in Figure 10.

The numerical results calculated in all scenarios for velocity, thermal gradient, and concentration are graphically portrayed in Figures 11–16 using interval [0, 5]. Figure 11 depicts that an increase in the electric field parameter (E_1) increases the fluid flow due to which the velocity $\widehat{g}'(\eta)$ of the fluid hikes. In actuality, the strength of the electric field increases, the charged particles in the nanofluid encounter an increased push directed towards the field. The charged particles are accelerated by this increased force, which raises the NF's velocity overall. Figure 12 explains that an uplift in the numeric value of the magnetic field parameter (M) resists in fluid flow which results in the form of velocity $\widehat{g}'(\eta)$ decay. The reason behind this decay is the increase of Lorentz force which is produced due to stronger magnetic force. Figure 13 portrays that the larger value of the mixed convection parameter (λ) enhances the nanofluidic flow which boosts the velocity $\widehat{g}'(\eta)$ of the fluid which is due to the rise in forced convection of fluid molecules along with nanoparticles over a stretchable surface. Figure 14 illustrates that a higher numeric value of buoyancy ratio parameter (N_1) increases the fluid flow

[**GA procedures**]
Inputs: The chromosomes utilized as evenly divided entries of network are expressed as $W = [W_g, W_\theta, W_\phi]$
Population: The vectors present in chromosomes are
$W_g = [\alpha_{1g}, \alpha_{2g}, \alpha_{3g}]$, $W_\theta = [\alpha_{1\theta}, \alpha_{2\theta}, \alpha_{3\theta}]$ and $W_\phi = [\alpha_{1\phi}, \alpha_{2\phi}, \alpha_{3\phi}]$
Output: Collection of best-attained weight vectors named $W_{\text{GA-BEST}}$
Initialization:
Formation of real entries-based vector W for selection of a chromosome to use in gaoptimset settings.
Fitness assessment: Establish fitness **E** in well versed form through equations (9)–(13)
Stopping parameter: Terminate the process if any of the following is obtained:
(i) [*Fitness* = 1e−21], [Population Size = 244], [Elite count = 41], [StallLimit = 101], [Generations = 444], [TolFun = TolCon = 1e−21],
(ii) Other values: using by default store the calculated results.
Ranking: **G**ain "E" via ranking W.
Reproduction:
[Selection⟶@stoch-uniform], [mutation⟶adapt-feasible], [Crossover⟶heuristic]
Store: Store the desired trained weights $W_{\text{GA-BEST}}$, **E**, time, generations as well as function counts.
GA process (**end**)
Process of SQP (**% start%**)
Inputs: Input $W_{\text{GA-BEST}}$
Output: Best collected weights through NHA-GA-SQP $W_{\text{GA-SQP}}$.
Initialize: Utilization of bounded constraints, assignments, generations along with $W_{\text{GA-BEST}}$.
Terminate: Procedure stops on attaining any of the following:
(iii) [e = 1e−21], [Iterations = 1544], [Tol_Con = Tol_X = Tol_Fun = 1e−21], [Max_Evals_Fun = 2100000].
(iv) Other settings (By default)
Fitness assessment: Estimate "E" through equations (9)–(13). Utilize "fmincon" for amendments and modifications
Accumulate:
Save $W_{\text{GA-SQP}}$, "E" along function count**,** time, and iterations.
SQP (**%end%**)
Data Generations
Hybrid function is repeated 20 times for nano viscous fluid problem through the NHA-GA-SQP algorithm to collect a large dataset

Algorithm 1: Pseudocode using NHA-GA-SQP algorithm for nano viscous fluid problem.

which results as an increase in the velocity $\widehat{g}'(\eta)$ of the nanofluid. The reason behind this increase is that a higher value of the buoyancy ratio parameter typically corresponds to a larger difference in density between the fluid and its surroundings. This density difference creates buoyancy and induces buoyancy-induced convection within the nanofluid. Stronger buoyancy promotes fluid movement, and as a result, velocity profile uplifts. Figure 15 describes that an escalation in the value of the Brownian motion parameter (N_b) amplifies the temperature gradient $\widehat{\theta}(\eta)$ of the fluid, and as a result, the concentration $\widehat{\phi}(\eta)$ of the base fluid, as well as the nanoparticles, diminishes. Figure 16 shows that in scenario 6, when the value of Schmidt number (S_c) rises, then it de-escalates the mass diffusivity which decreases the concentration $\widehat{\phi}(\eta)$ of the NF. In case of scenario 7, the effect of the reaction parameter (γ) on NF is the same as that of S_c in scenario 6. It is due to the fact that an increase in a chemical reaction parameter may indicate that the nanoparticles in the nanofluid are undergoing more chemical reactions at a faster rate. An increased reaction parameter would cause a more substantial depletion of nanoparticles, which would lower the concentration.

The NHA-GA-SQP algorithm produces the numerical results of the nano viscous fluid problem that overlaps the reference solution quite significantly in each scenario using interval [0, 5]. This statement is verified through absolute errors (AEs) that depict graphically in Figure 17, and its tabulated form is represented in Table 2. The calculated range of AEs is 10^{-3}–10^{-6} for 1st two scenarios, 10^{-3}–10^{-7} for 3rd and 4th scenarios, 10^{-3}–10^{-6} for 5th and 7th scenarios, while this range is 10^{-3}–10^{-7} for 6th scenario.

The performance of the NHA-GA-SQP algorithm is analyzed through distinct statistical performance operators, while the obtained data which is in shape of graphs are illustrated through Figures 18–26. All seven scenarios are randomly discussed through these operators, and these performance grades have ranges up to 10^{-4} for RMSE, up to 10^{-5} for E-TIC, up to 10^{-6} for both E-NSE and E-R^2, and up to 10^{-8} for E-VAF. These obtained values are very nearly equal to zero which proves the suitability and efficiency of the NHA-GA-SQP algorithm for the current problem. In the tabulated form, the performance of these statistical operators along with the best iteration number for all scenarios is presented in Table 3.

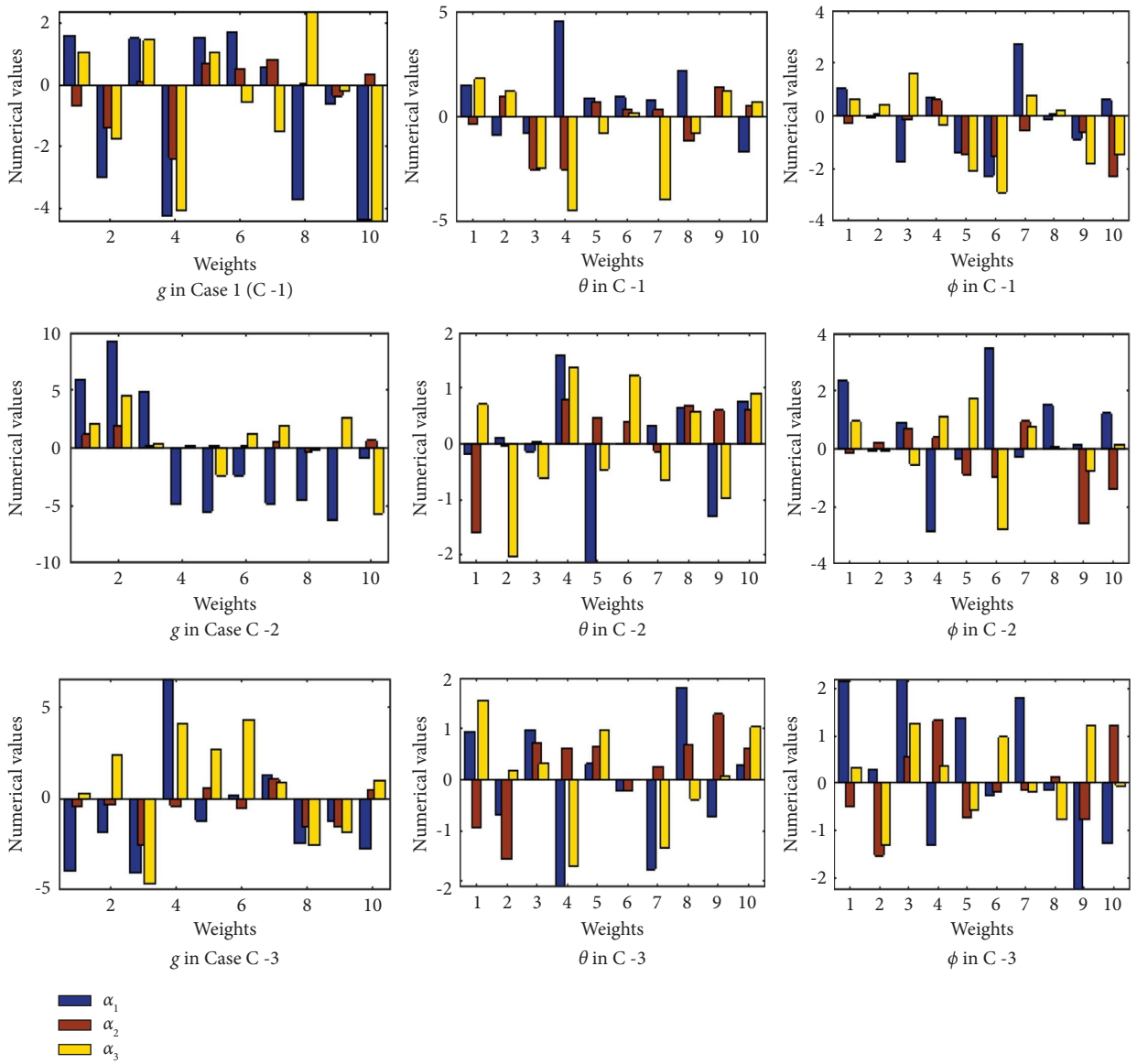

Figure 3: Best trained weights of the suggested nanofluidic problem for cases (1–3) of scenario 1 (S-I).

The proposed solver fitness is testified for some randomly taken scenarios through box-plot analysis and CDF-analysis which are portrayed in Figures 27 and 28 which also prove the reliability of the NHA-GA-SQP algorithm. Moreover, the convergence analysis based on fitness estimation for all seven scenarios is presented in Figure 29 which proves that the NHA-GA-SQP solver can attain the stiff criteria quite comfortably.

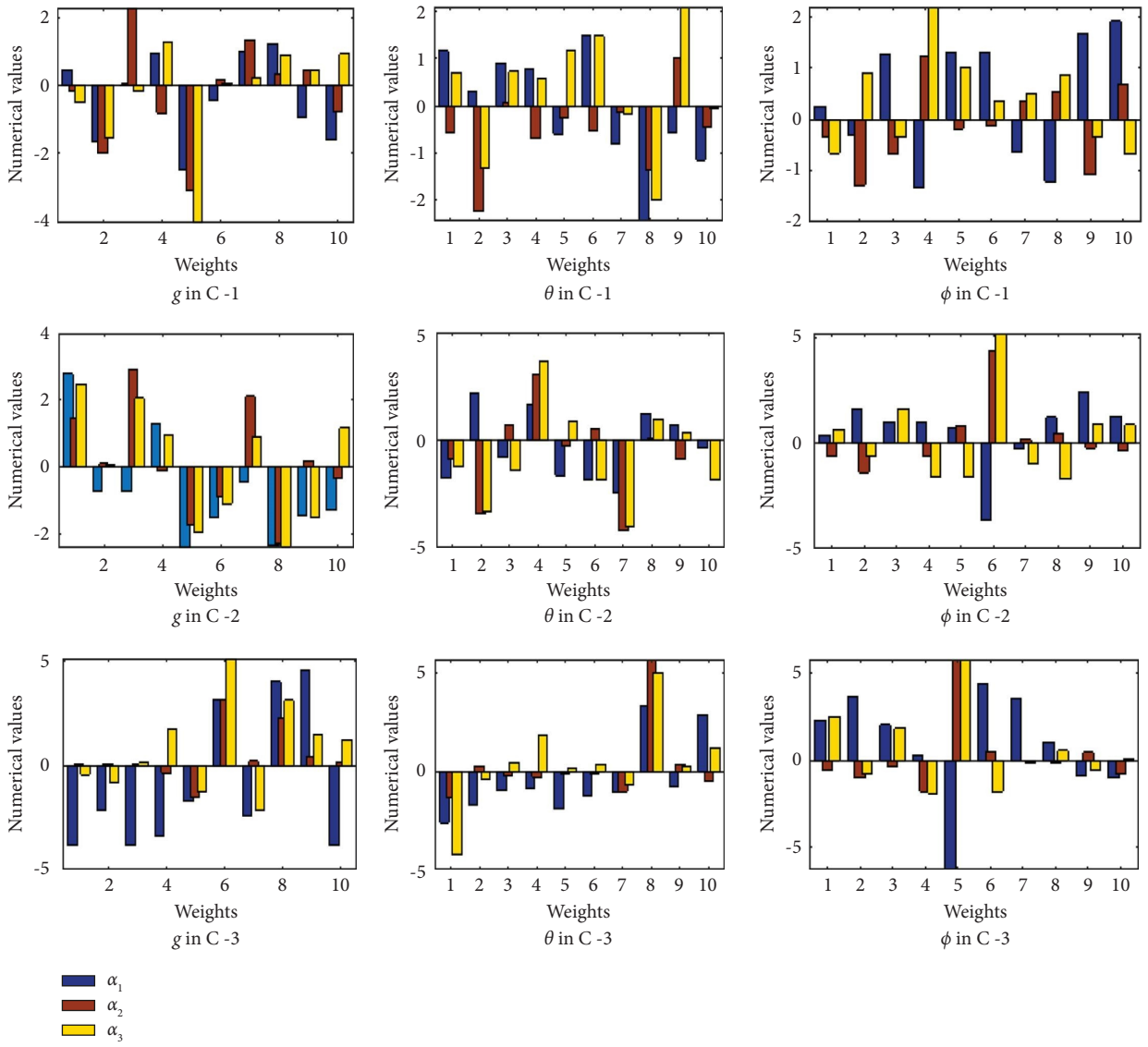

Figure 4: Best trained weights of the suggested nanofluidic problem for cases (1–3) of scenario 1 (S-II).

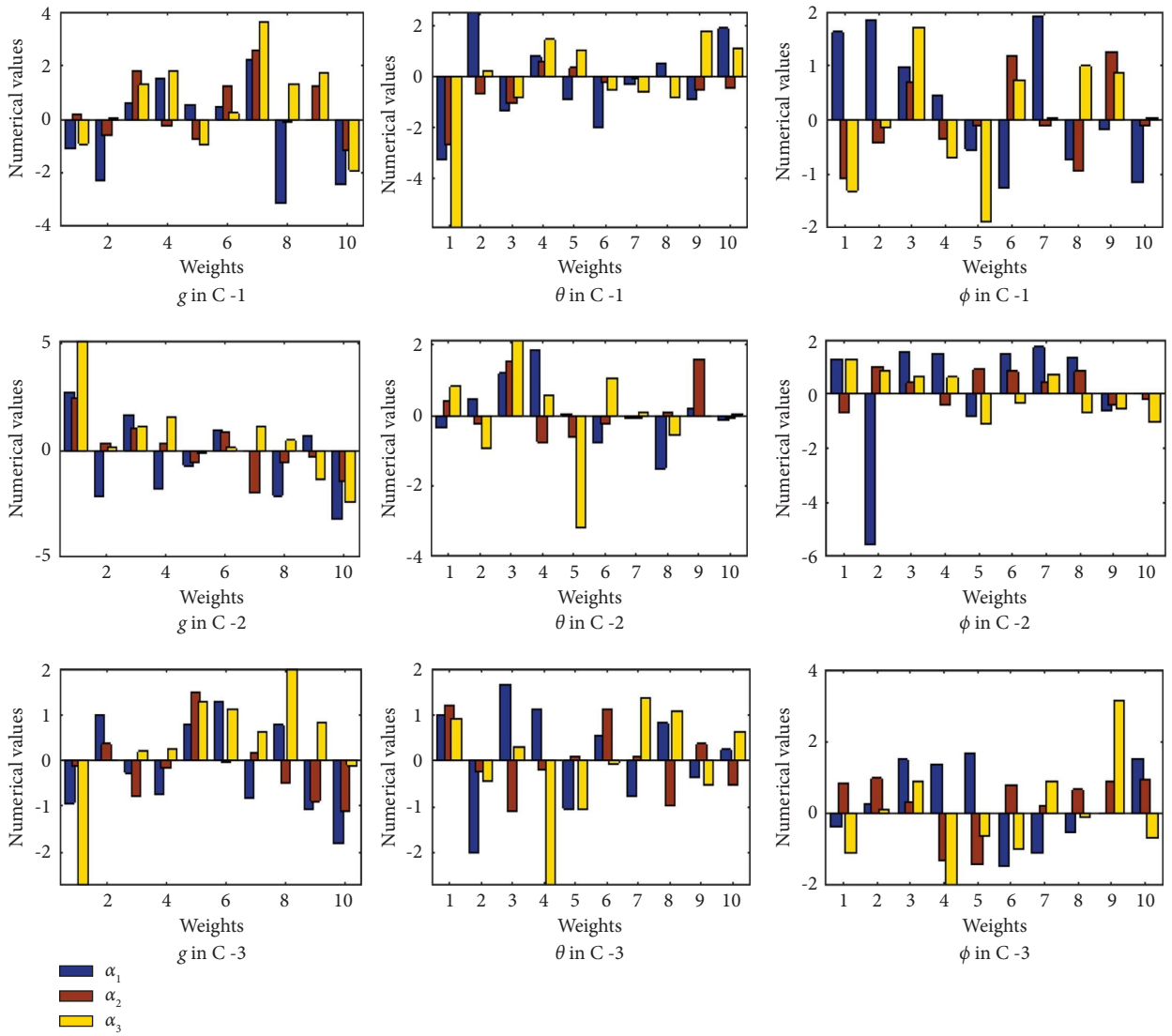

Figure 5: Best trained weights of the suggested nanofluidic problem for cases (1–3) of scenario 1 (S-III).

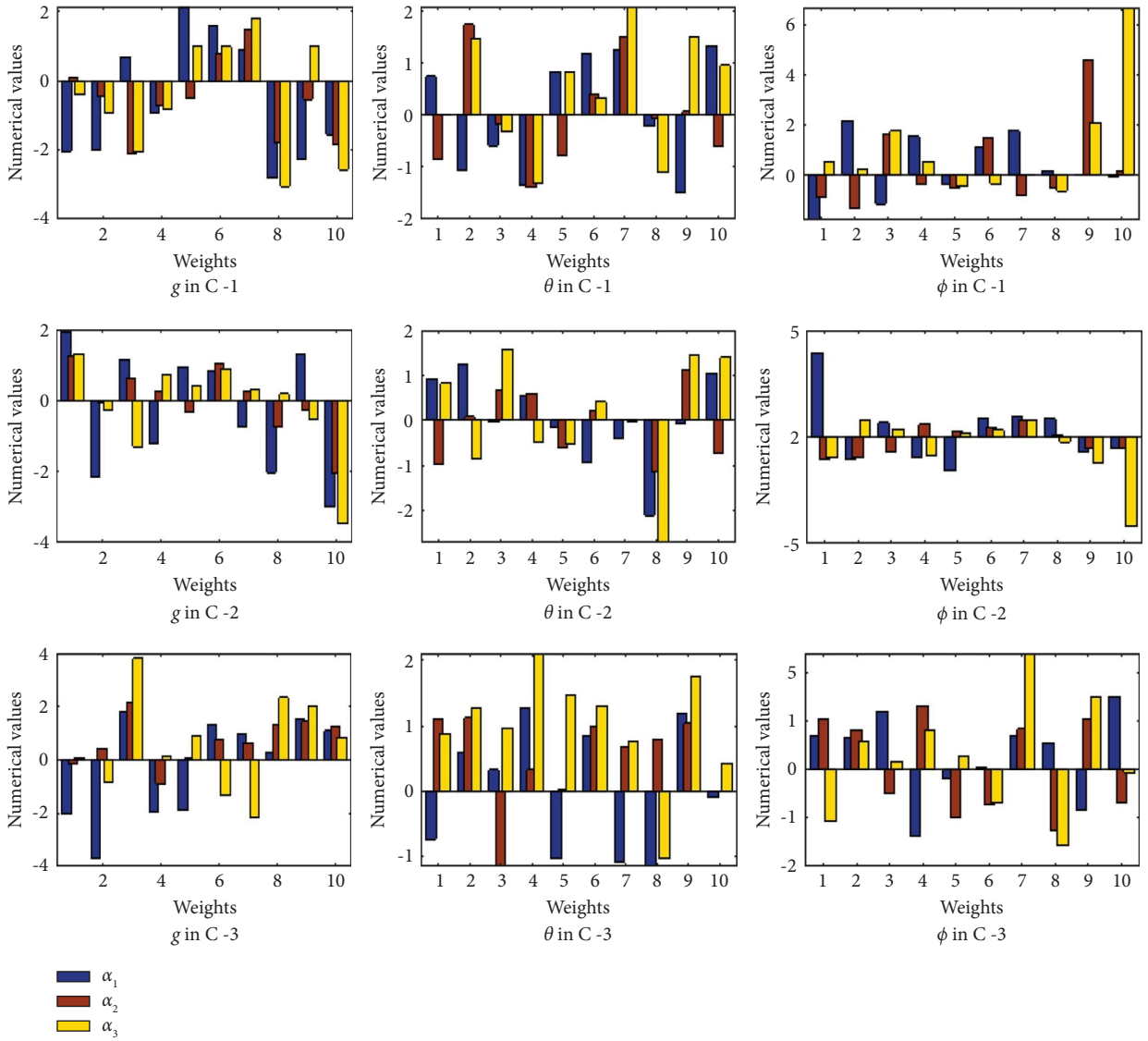

Figure 6: Best trained weights of the suggested nanofluidic problem for cases (1–3) of scenario 1 (S-IV).

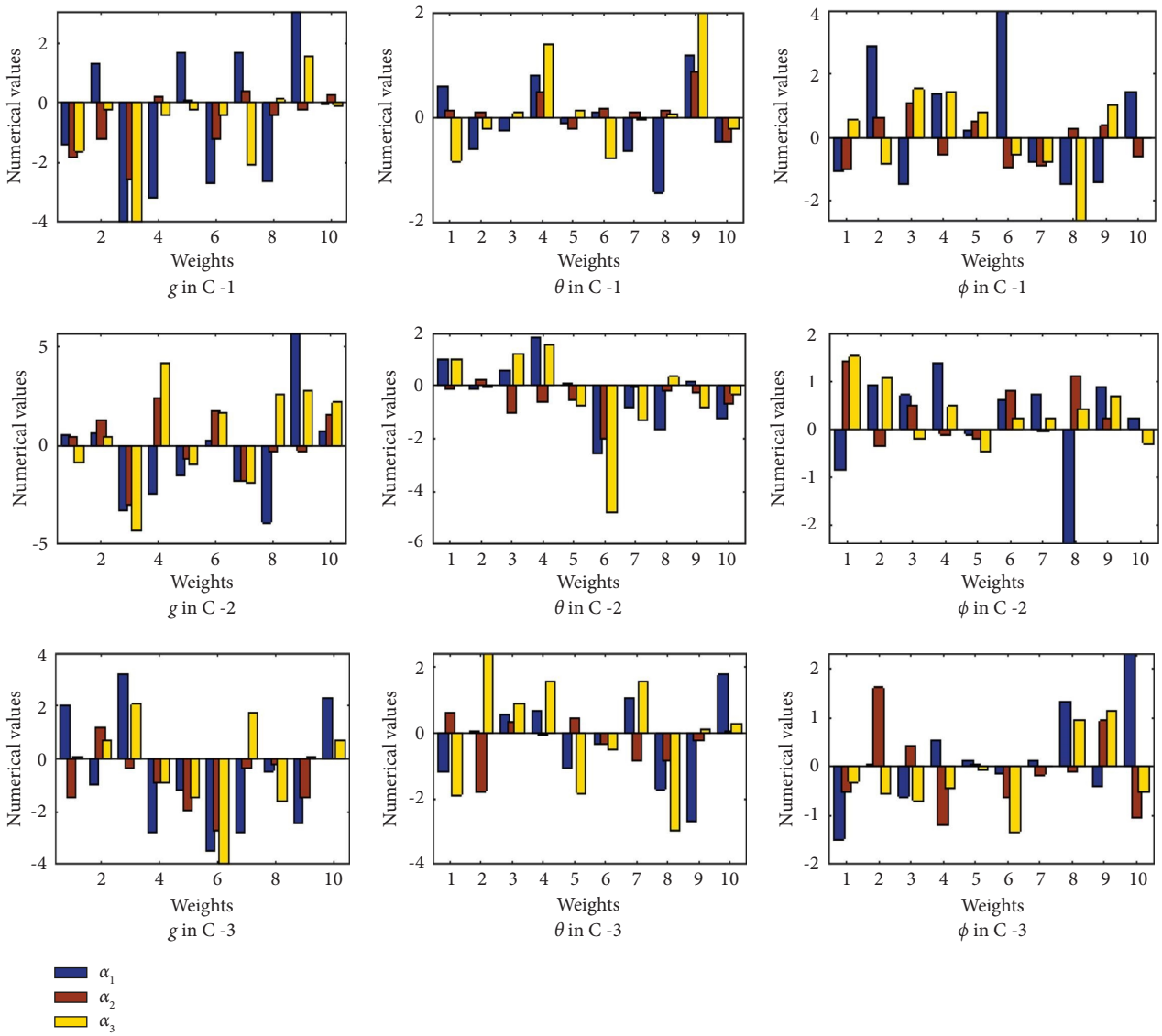

Figure 7: Best trained weights of the suggested nanofluidic problem for cases (1–3) of scenario 1 (S-V).

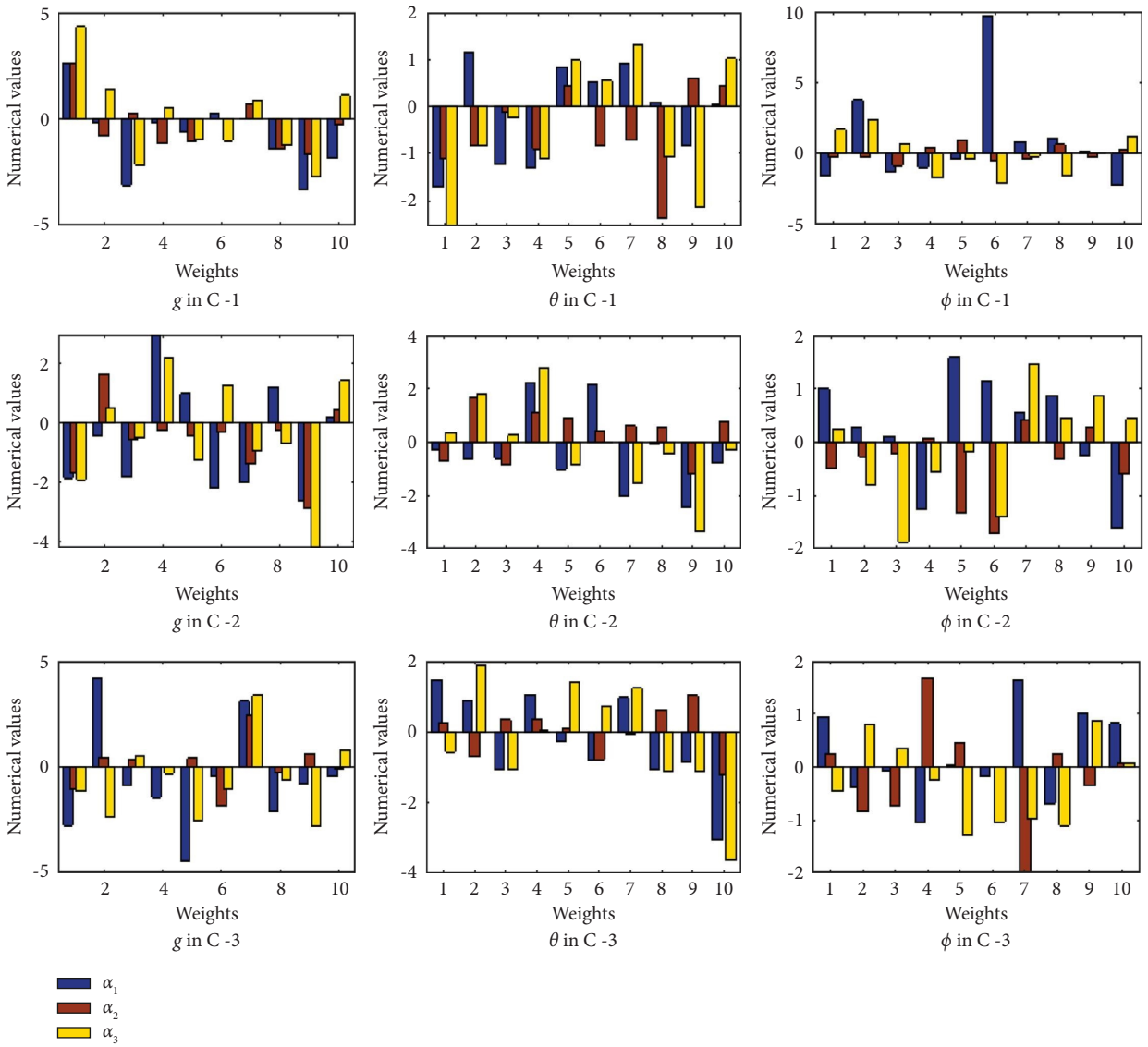

Figure 8: Best trained weights of the suggested nanofluidic problem for cases (1–3) of scenario 1 (S-VI).

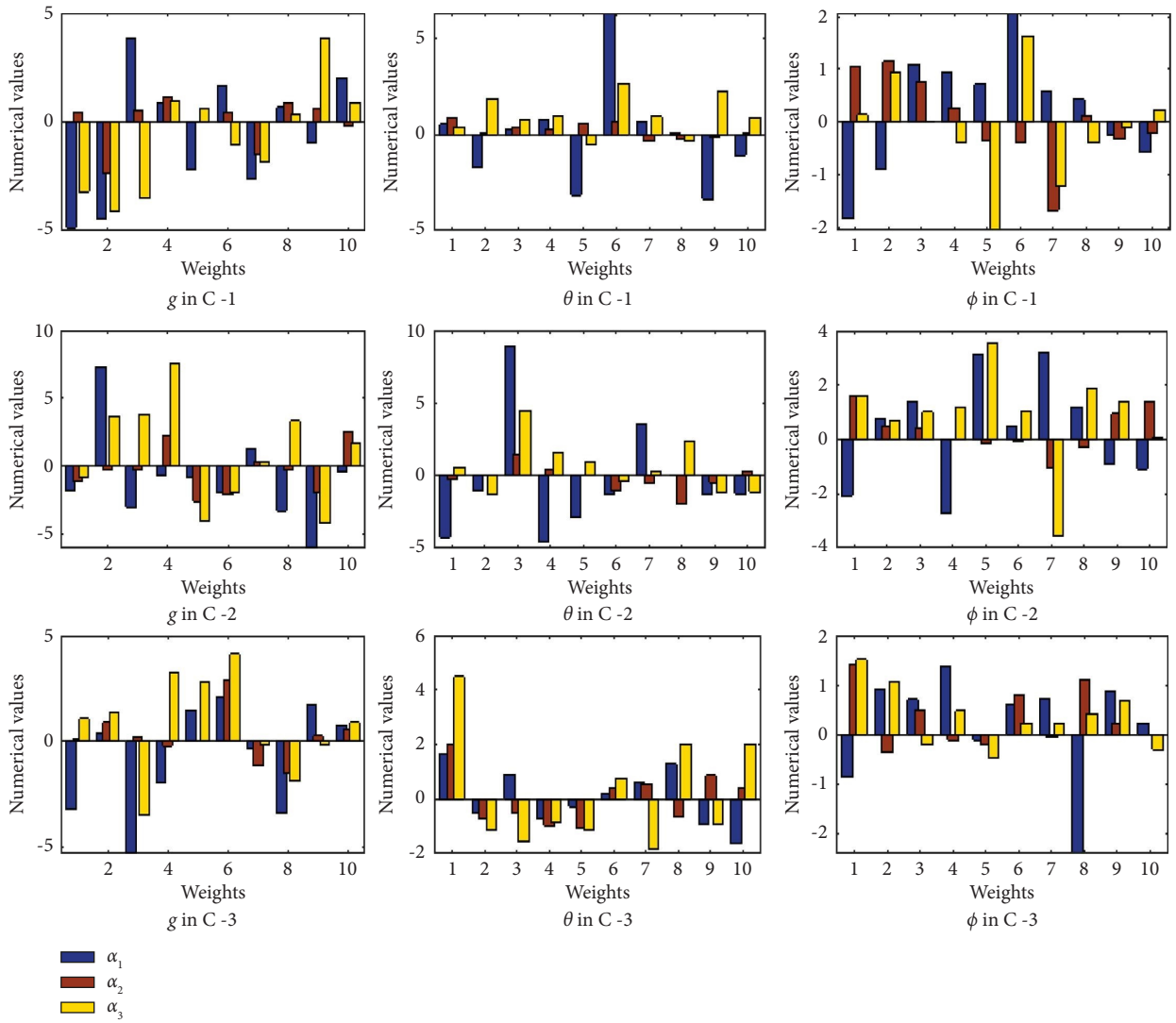

Figure 9: Best trained weights of the suggested nanofluidic problem for cases (1–3) of scenario 1 (S-VII).

Table 1: Values of physical parameters in three cases of all scenarios to solve the nano viscous fluid problem.

Cases	Scenarios						
	1	2	3	4	5	6	7
1	$E_1 = 0.3$	$M = 0.1$	$\lambda = 0.2$	$N_1 = 1.0$	$N_b = 0.4$	$S_c = 0.2$	$\gamma = 0.1$
2	$E_1 = 0.7$	$M = 0.3$	$\lambda = 0.4$	$N_1 = 2.0$	$N_b = 0.8$	$S_c = 0.8$	$\gamma = 0.7$
3	$E_1 = 1.0$	$M = 0.5$	$\lambda = 0.9$	$N_1 = 3.0$	$N_b = 1.5$	$S_c = 1.4$	$\gamma = 1.3$

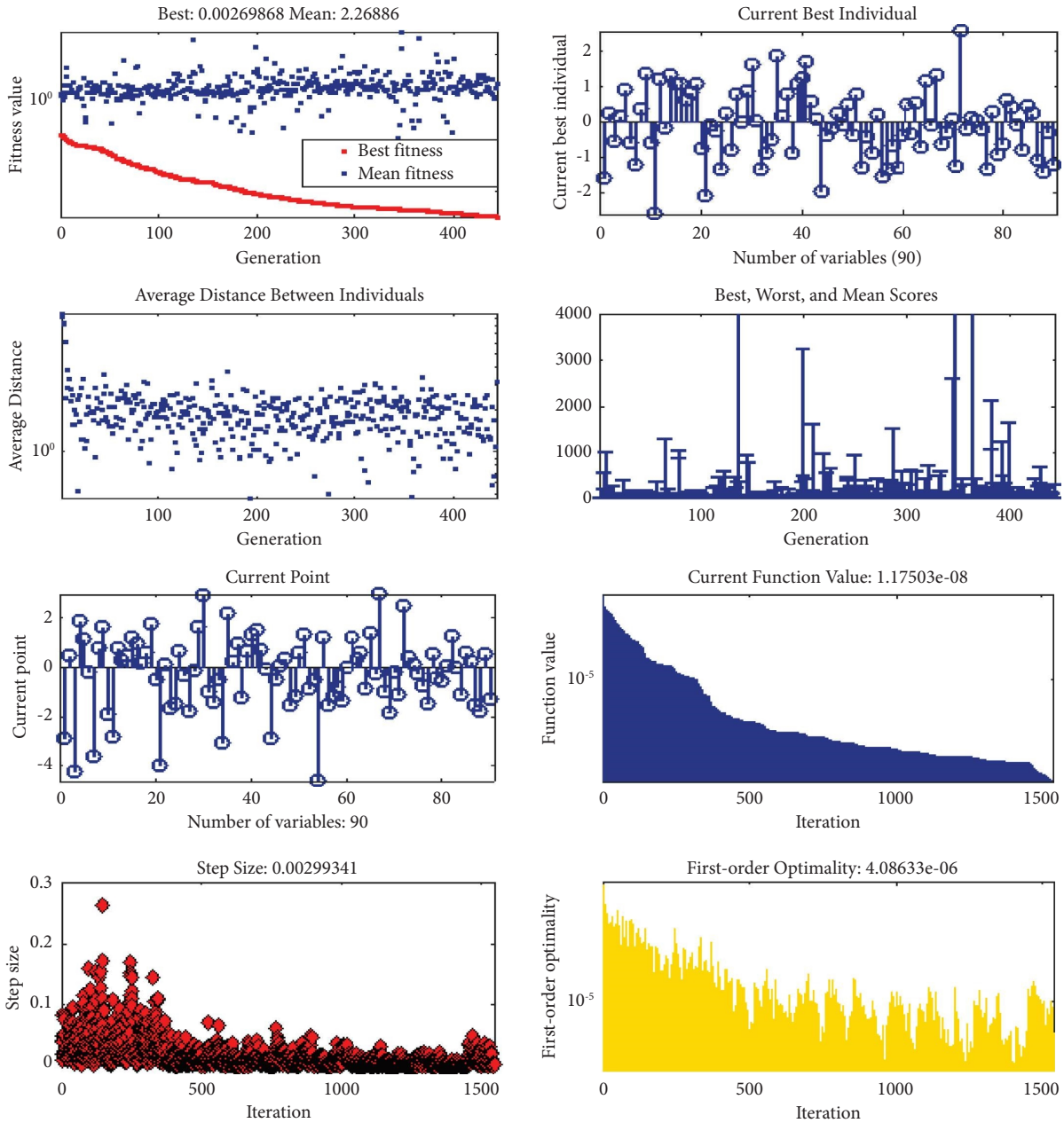

Figure 10: Learning curves obtained using NHA-GA-SQP in 1st case of scenario 1 for best weights' training.

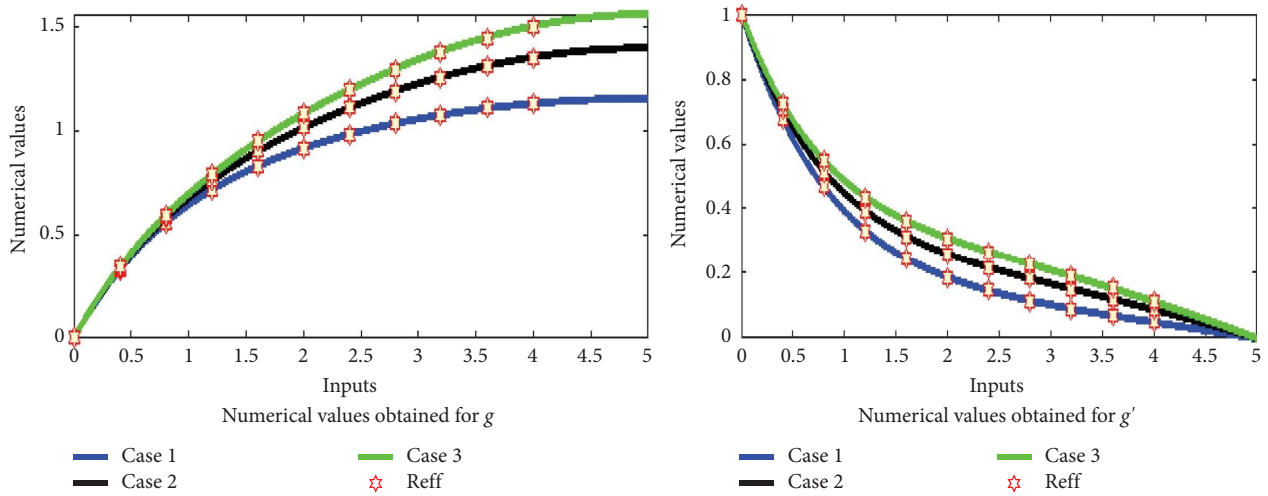

Figure 11: Numerical values obtained in the suggested nanofluidic problem for cases (1–3) of scenario 1 (S-I).

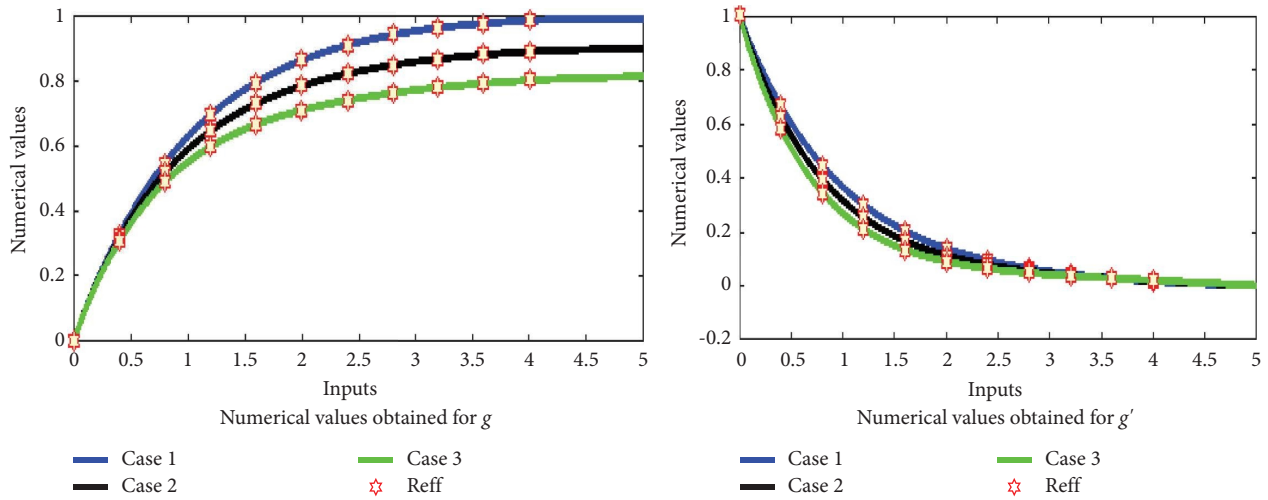

Figure 12: Numerical values obtained in the suggested nanofluidic problem for cases (1–3) of S-II.

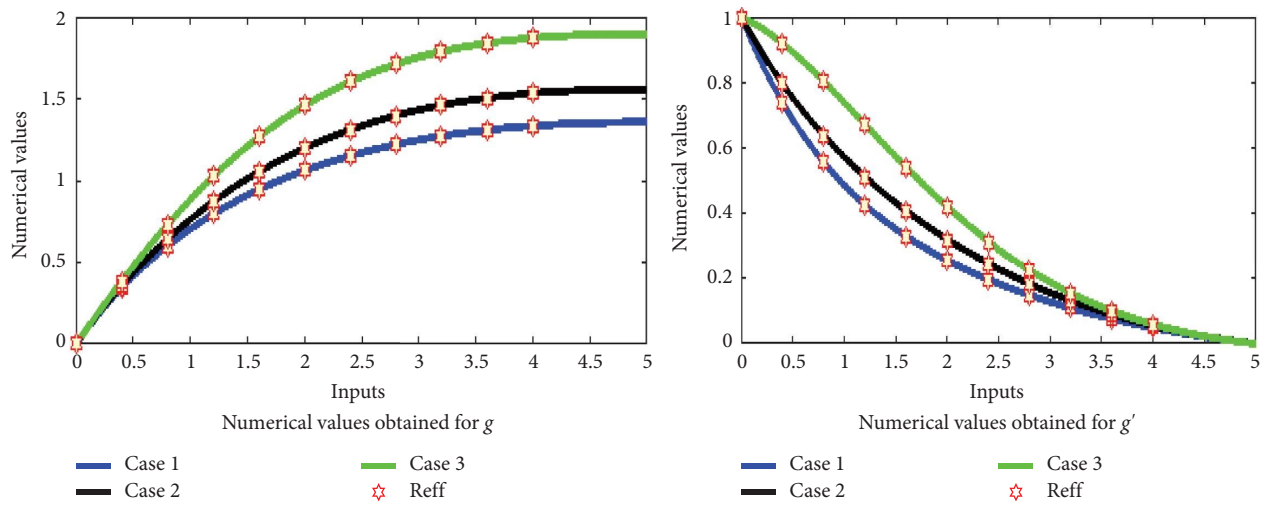

Figure 13: Numerical values obtained in the suggested nanofluidic problem for cases (1–3) of S-III.

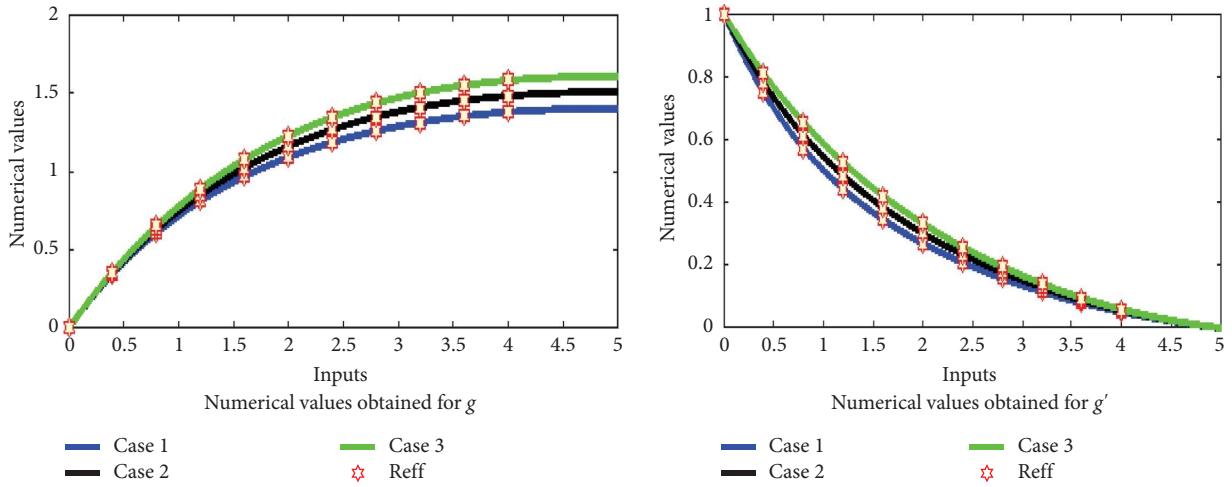

Figure 14: Numerical values obtained in the suggested nanofluidic problem for cases (1–3) of S-IV.

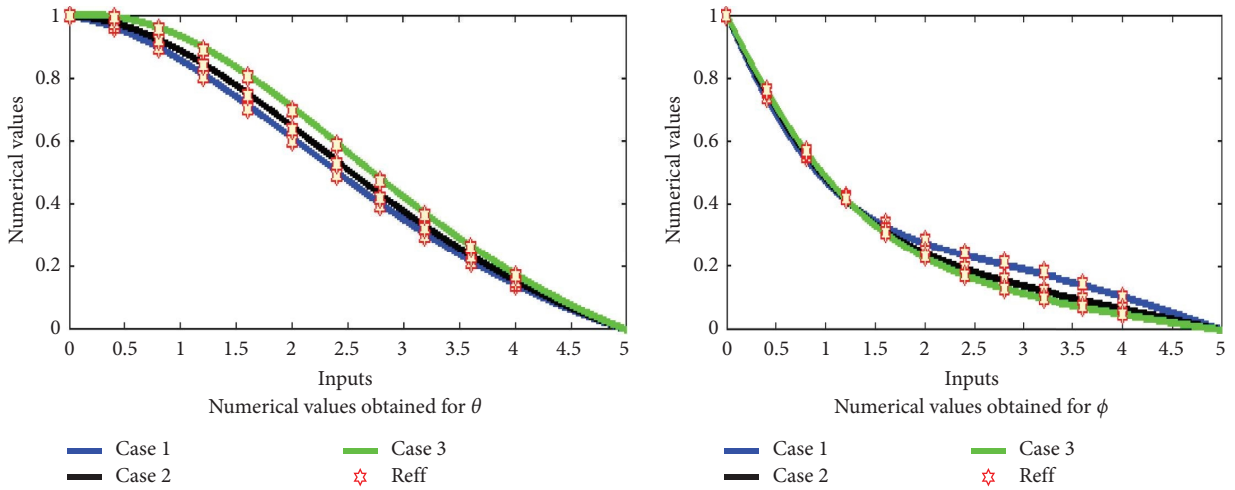

Figure 15: Numerical values obtained in the suggested nanofluidic problem for cases (1–3) of S-V.

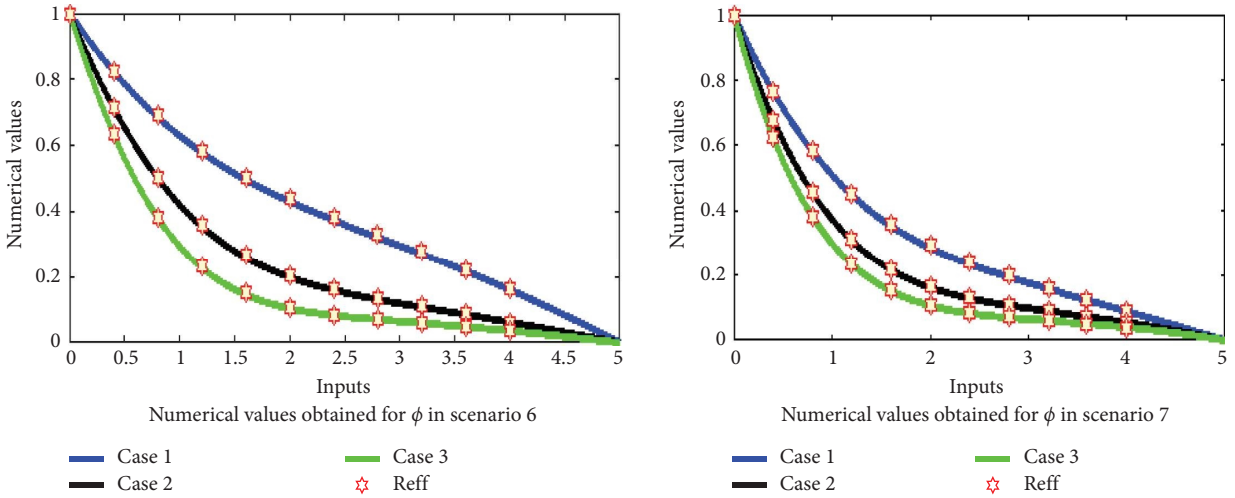

Figure 16: Numerical values obtained in the suggested nanofluidic problem for cases (1–3) of S (VI–VII).

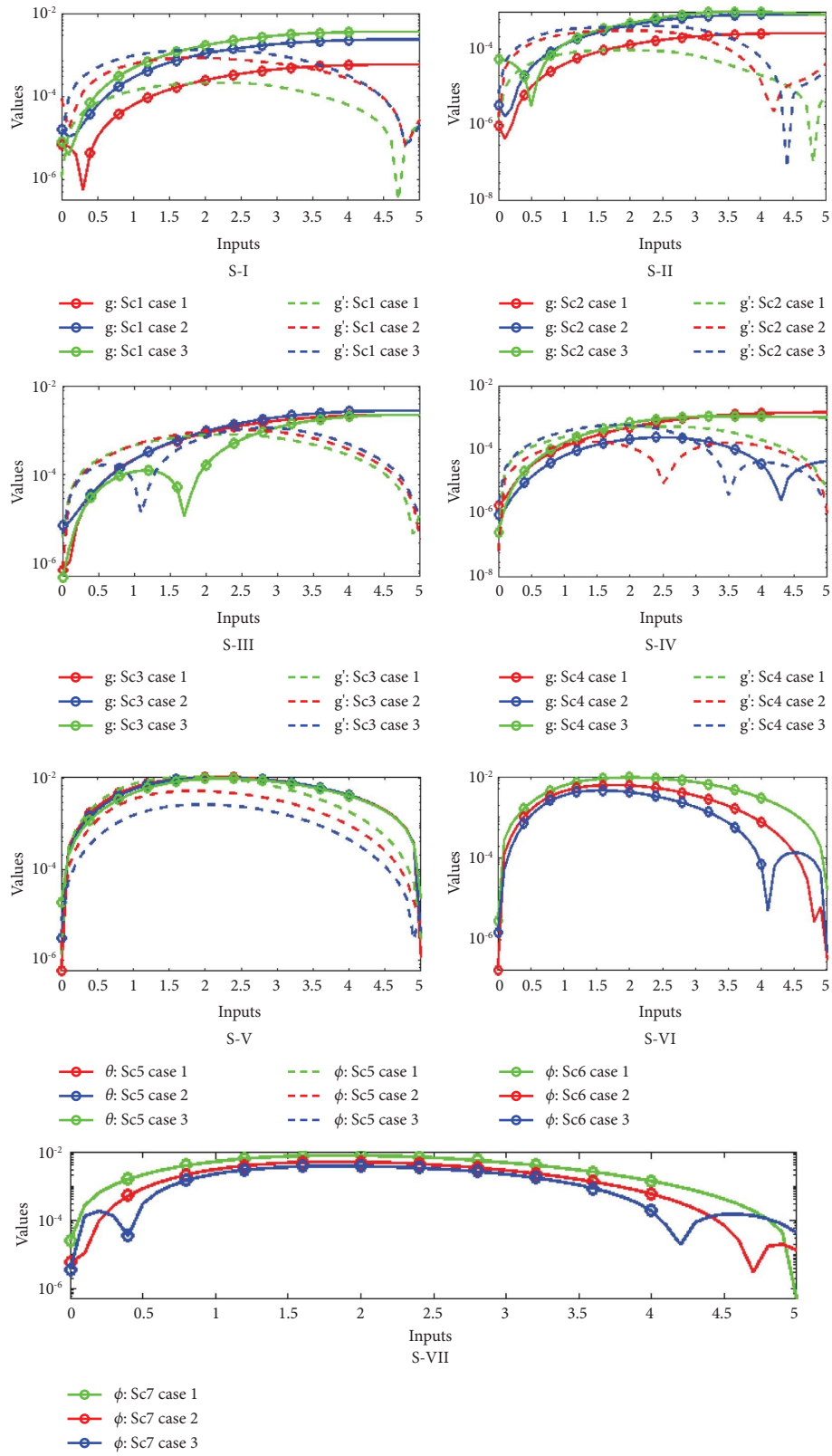

Figure 17: Values of absolute errors calculated in the nano viscous fluid problem in all scenarios.

Table 2: Absolute errors (AEs) computed in the suggested nanofluidic problem for S (I–VII).

η	Θ			ϕ		
	C − 1	C − 2	C − 3	C − 1	C − 2	C − 3
S-I						
0	$3.902E-6$	$3.697E-6$	$3.038E-6$	$3.061E-6$	$1.742E-5$	$1.024E-5$
0.5	$1.605E-5$	$7.451E-5$	$1.234E-4$	$7.241E-5$	$3.114E-4$	$5.061E-4$
1.0	$7.036E-5$	$3.040E-4$	$4.927E-4$	$1.441E-4$	$5.983E-4$	$9.548E-4$
1.5	$1.577E-4$	$6.591E-4$	$1.053E-3$	$2.019E-4$	$8.018E-4$	$1.252E-3$
2.0	$2.679E-4$	$1.082E-3$	$1.709E-3$	$2.333E-4$	$8.676E-4$	$1.337E-3$
2.5	$3.852E-4$	$1.506E-3$	$2.359E-3$	$2.299E-4$	$8.111E-4$	$1.237E-3$
3.0	$4.925E-4$	$1.879E-3$	$2.921E-3$	$1.955E-4$	$6.671E-4$	$9.920E-4$
3.5	$5.780E-4$	$2.164E-3$	$3.337E-3$	$1.452E-4$	$4.680E-4$	$6.663E-4$
4.0	$6.375E-4$	$2.345E-3$	$3.589E-3$	$9.300E-5$	$2.605E-4$	$3.501E-4$
4.5	$6.713E-4$	$2.432E-3$	$3.702E-3$	$4.279E-5$	$9.424E-5$	$1.173E-4$
5.0	$6.815E-4$	$2.452E-3$	$3.726E-3$	$5.815E-6$	$5.622E-6$	$4.257E-6$
S-II						
0	$1.707E-6$	$1.753E-6$	$4.326E-6$	$1.984E-6$	$1.580E-6$	$3.565E-6$
0.5	$1.153E-5$	$3.388E-5$	$4.371E-5$	$4.317E-5$	$1.376E-4$	$1.792E-4$
1.0	$4.171E-5$	$1.307E-4$	$1.686E-4$	$7.579E-5$	$2.411E-4$	$3.116E-4$
1.5	$8.551E-5$	$2.683E-4$	$3.436E-4$	$9.681E-5$	$3.018E-4$	$3.772E-4$
2.0	$1.355E-4$	$4.236E-4$	$5.367E-4$	$1.004E-4$	$3.114E-4$	$3.883E-4$
2.5	$1.838E-4$	$5.739E-4$	$7.260E-4$	$9.155E-5$	$2.856E-4$	$3.636E-4$
3.0	$2.263E-4$	$7.054E-4$	$8.948E-4$	$7.818E-5$	$2.363E-4$	$3.063E-4$
3.5	$2.617E-4$	$8.060E-4$	$1.027E-3$	$6.253E-5$	$1.628E-4$	$2.166E-4$
4.0	$2.881E-4$	$8.670E-4$	$1.108E-3$	$4.222E-5$	$8.260E-5$	$1.270E-4$
4.5	$3.032E-4$	$8.927E-4$	$1.141E-3$	$1.813E-5$	$2.893E-5$	$5.333E-5$
5.0	$3.073E-4$	$8.971E-4$	$1.142E-3$	$3.447E-6$	$9.206E-6$	$2.236E-5$
S-III						
0	$2.631E-6$	$1.493E-6$	$6.075E-7$	$1.675E-6$	$1.248E-6$	$7.777E-7$
0.5	$5.387E-5$	$4.899E-5$	$4.380E-5$	$2.229E-4$	$2.004E-4$	$1.556E-4$
1.0	$2.248E-4$	$2.129E-4$	$1.151E-4$	$4.611E-4$	$4.667E-4$	$8.028E-5$
1.5	$5.097E-4$	$5.204E-4$	$7.665E-5$	$6.680E-4$	$7.586E-4$	$2.718E-4$
2.0	$8.779E-4$	$9.578E-4$	$1.748E-4$	$7.870E-4$	$9.703E-4$	$7.297E-4$
2.5	$1.277E-3$	$1.465E-3$	$6.289E-4$	$7.912E-4$	$1.033E-3$	$1.048E-3$
3.0	$1.650E-3$	$1.963E-3$	$1.177E-3$	$6.842E-4$	$9.298E-4$	$1.095E-3$
3.5	$1.949E-3$	$2.373E-3$	$1.681E-3$	$5.006E-4$	$6.955E-4$	$8.875E-4$
4.0	$2.147E-3$	$2.649E-3$	$2.041E-3$	$2.949E-4$	$4.085E-4$	$5.409E-4$
4.5	$2.249E-3$	$2.788E-3$	$2.225E-3$	$1.182E-4$	$1.590E-4$	$2.102E-4$
5.0	$2.275E-3$	$2.824E-3$	$2.272E-3$	$3.658E-6$	$1.632E-6$	$1.763E-6$
S-IV						
0	$1.024E-6$	$9.894E-7$	$2.346E-6$	$7.744E-7$	$7.420E-7$	$2.459E-6$
0.5	$2.970E-5$	$1.572E-5$	$3.458E-5$	$1.204E-4$	$6.415E-5$	$1.527E-4$
1.0	$1.225E-4$	$6.774E-5$	$1.654E-4$	$2.531E-4$	$1.427E-4$	$3.766E-4$
1.5	$2.834E-4$	$1.505E-4$	$4.038E-4$	$3.884E-4$	$1.744E-4$	$5.572E-4$
2.0	$5.059E-4$	$2.268E-4$	$6.944E-4$	$4.936E-4$	$1.167E-4$	$5.730E-4$
2.5	$7.665E-4$	$2.573E-4$	$9.476E-4$	$5.364E-4$	$3.698E-6$	$4.175E-4$
3.0	$1.029E-3$	$2.273E-4$	$1.099E-3$	$5.008E-4$	$1.153E-4$	$1.877E-4$
3.5	$1.255E-3$	$1.523E-4$	$1.144E-3$	$3.930E-4$	$1.709E-4$	$6.593E-6$
4.0	$1.415E-3$	$7.043E-5$	$1.125E-3$	$2.443E-4$	$1.441E-4$	$6.365E-5$
4.5	$1.500E-3$	$1.939E-5$	$1.095E-3$	$1.011E-4$	$6.980E-5$	$4.580E-5$
5.0	$1.523E-3$	$1.363E-5$	$1.083E-3$	$1.648E-6$	$2.509E-6$	$1.971E-6$
S-V						
η	Θ			ϕ		
	C − 1	C − 2	C − 3	C − 1	C − 2	C − 3
0	$2.147E-6$	$2.884E-6$	$4.009E-6$	$2.191E-6$	$2.318E-6$	$2.054E-6$
0.5	$2.401E-3$	$2.061E-3$	$1.549E-3$	$2.841E-3$	$1.222E-3$	$4.922E-4$
1.0	$6.297E-3$	$5.807E-3$	$4.990E-3$	$7.527E-3$	$3.513E-3$	$1.649E-3$
1.5	$9.376E-3$	$8.917E-3$	$8.137E-3$	$1.045E-2$	$5.055E-3$	$2.525E-3$
2.0	$1.071E-2$	$1.035E-2$	$9.767E-3$	$1.071E-2$	$5.271E-3$	$2.738E-3$
2.5	$1.042E-2$	$1.018E-2$	$9.802E-3$	$9.075E-3$	$4.528E-3$	$2.419E-3$
3.0	$8.956E-3$	$8.825E-3$	$8.605E-3$	$6.565E-3$	$3.332E-3$	$1.816E-3$

Table 2: Continued.

η	Θ			ϕ		
	C – 1	C – 2	C – 3	C – 1	C – 2	C – 3
3.5	$6.792E-3$	$6.732E-3$	$6.618E-3$	$3.996E-3$	$2.071E-3$	$1.147E-3$
4.0	$4.362E-3$	$4.331E-3$	$4.286E-3$	$1.896E-3$	$1.008E-3$	$5.674E-4$
4.5	$2.017E-3$	$2.004E-3$	$1.994E-3$	$5.384E-4$	$2.976E-4$	$1.745E-4$
5.0	$4.285E-6$	$5.824E-6$	$6.963E-6$	$6.572E-6$	$3.199E-6$	$2.847E-6$
	S-VI			S-VII		
η	ϕ			ϕ		
	C – 1	C – 2	C – 3	C – 1	C – 2	C – 3
0	$3.696E-6$	$1.846E-6$	$9.660E-7$	$1.959E-6$	$4.418E-6$	$4.091E-6$
0.5	$2.338E-3$	$1.552E-3$	$1.139E-3$	$2.071E-3$	$8.313E-4$	$3.081E-4$
1.0	$6.067E-3$	$4.407E-3$	$3.489E-3$	$5.375E-3$	$3.201E-3$	$2.246E-3$
1.5	$8.805E-3$	$6.126E-3$	$4.614E-3$	$7.510E-3$	$4.818E-3$	$3.600E-3$
2.0	$9.706E-3$	$6.135E-3$	$4.230E-3$	$7.756E-3$	$5.001E-3$	$3.751E-3$
2.5	$9.058E-3$	$5.016E-3$	$3.078E-3$	$6.637E-3$	$4.203E-3$	$3.133E-3$
3.0	$7.400E-3$	$3.460E-3$	$1.809E-3$	$4.874E-3$	$2.983E-3$	$2.172E-3$
3.5	$5.258E-3$	$1.964E-3$	$7.805E-4$	$3.039E-3$	$1.724E-3$	$1.150E-3$
4.0	$3.099E-3$	$8.188E-4$	$1.328E-4$	$1.502E-3$	$6.972E-4$	$3.263E-4$
4.5	$1.283E-3$	$1.583E-4$	$1.116E-4$	$4.647E-4$	$1.048E-4$	$7.199E-5$
5.0	$7.038E-6$	$1.871E-6$	$4.220E-6$	$4.076E-6$	$5.292E-6$	$2.142E-5$

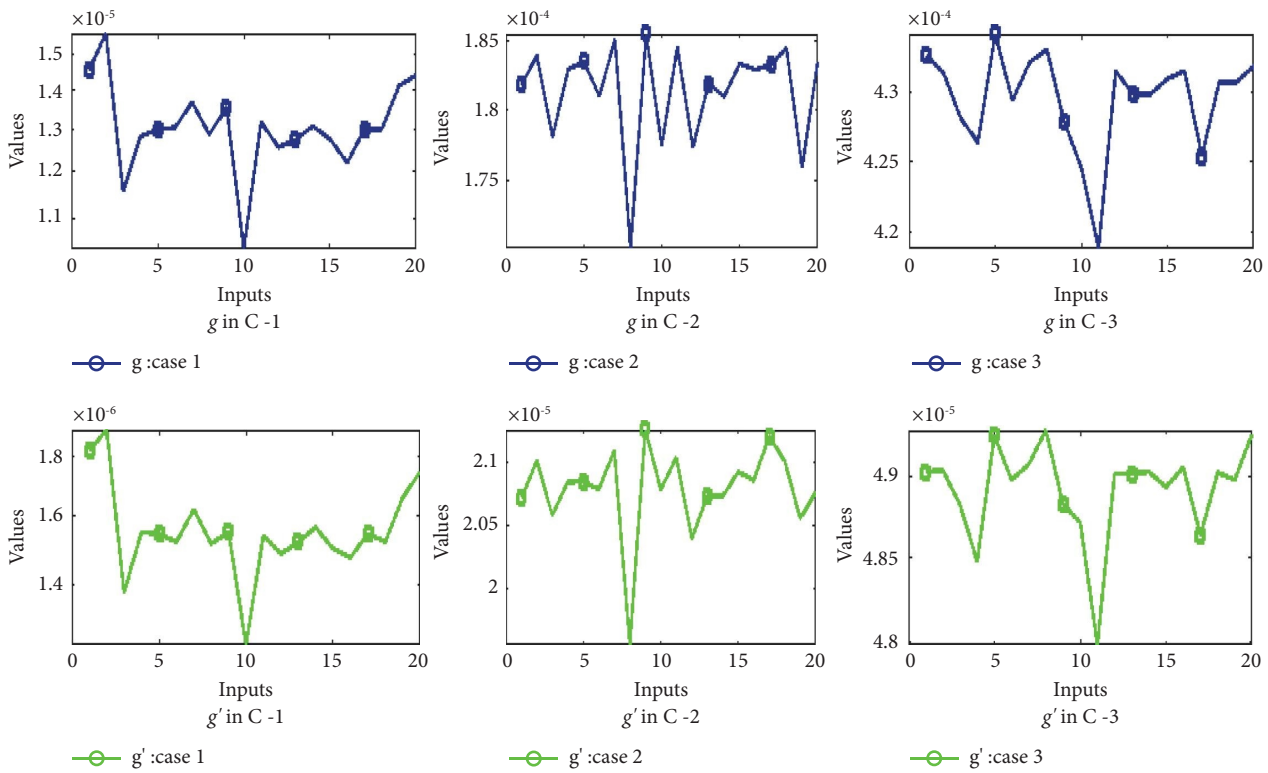

Figure 18: E-R^2 analysis for the nano viscous fluid problem in S-I.

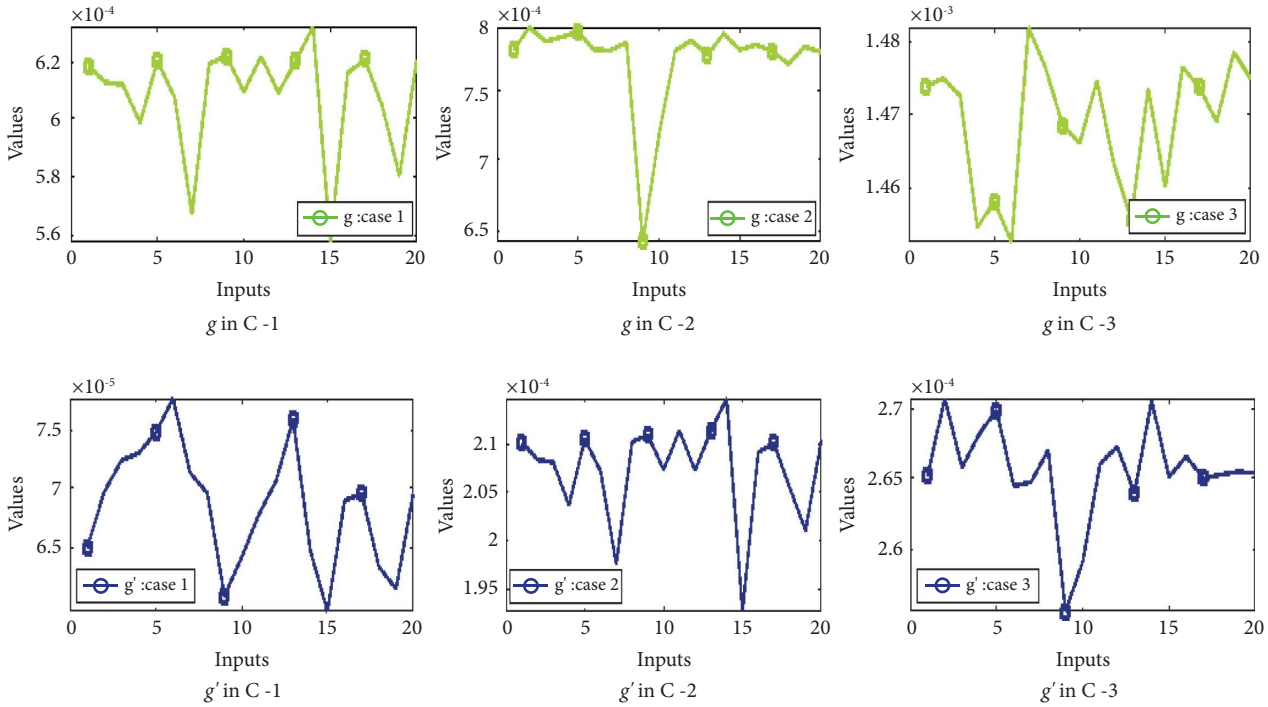

Figure 19: RMSE analysis for the nano viscous fluid problem in S-II.

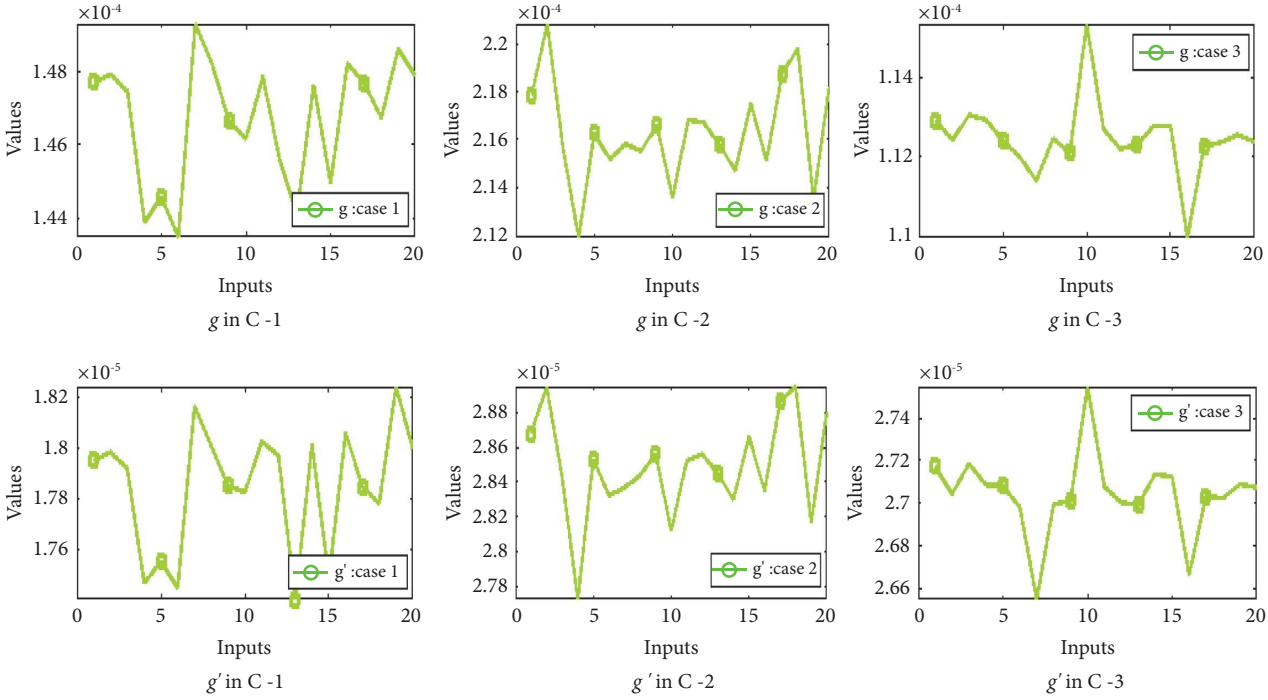

Figure 20: E-NSE analysis for the nano viscous fluid problem in S-III.

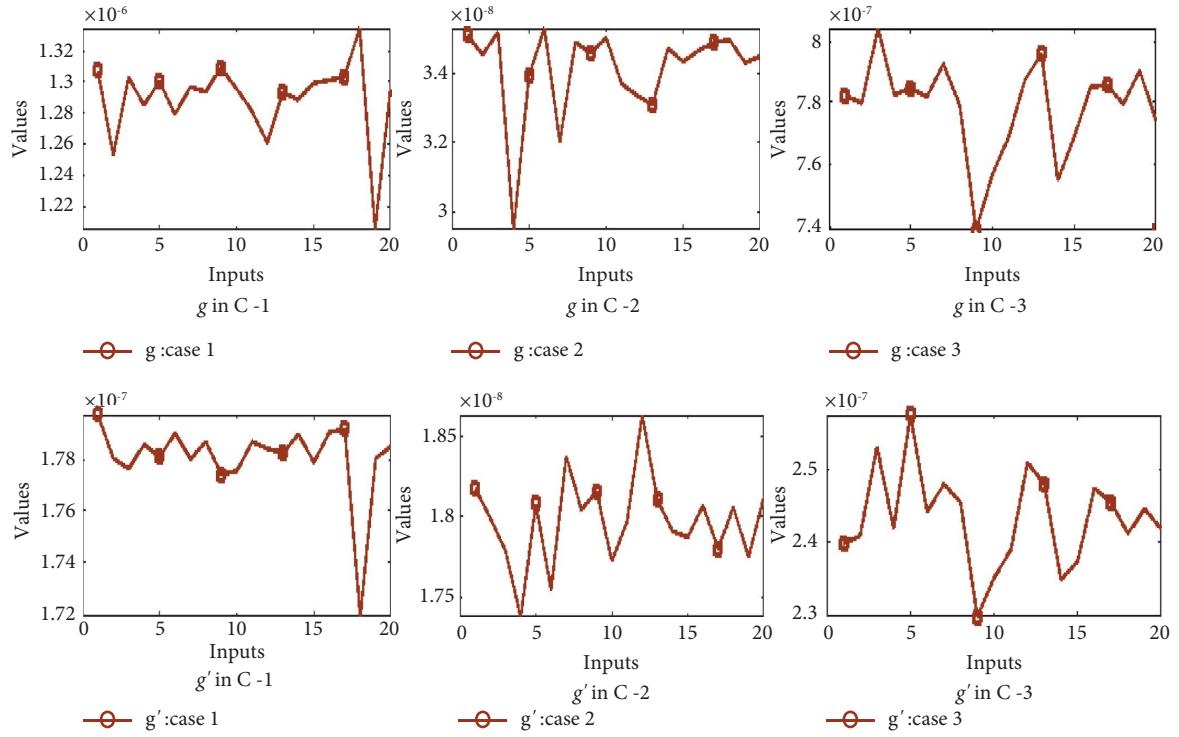

Figure 21: E-VAF analysis for the nano viscous fluid problem in S-IV.

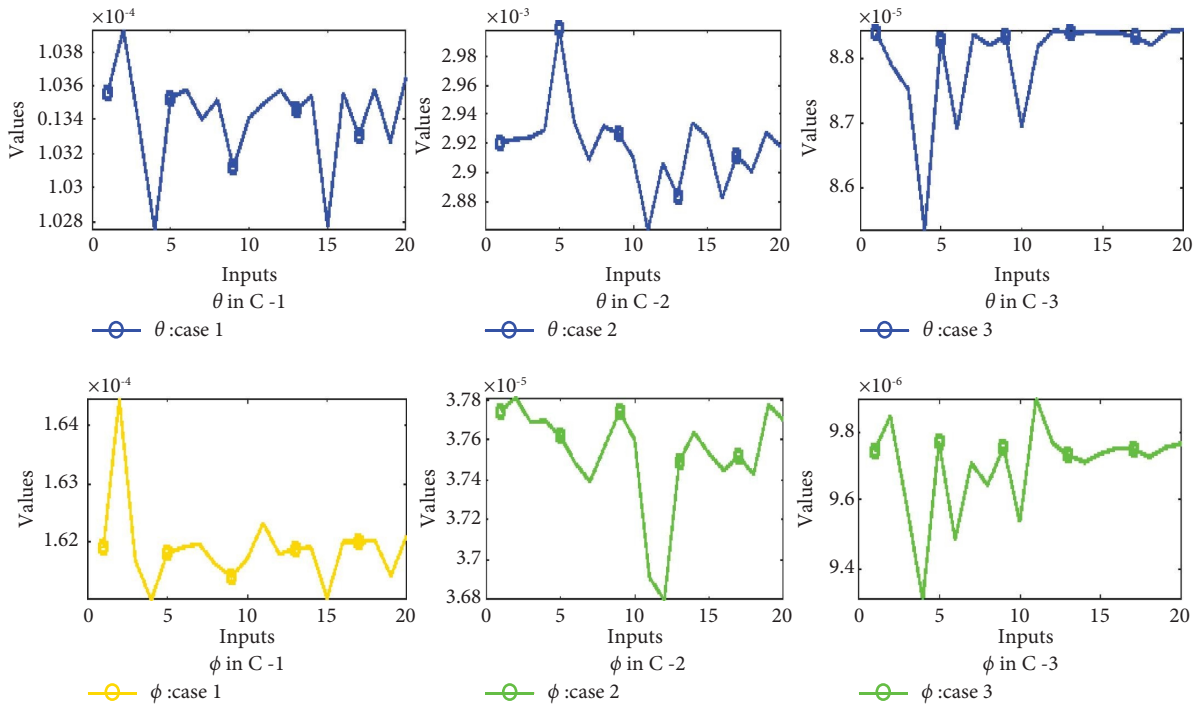

Figure 22: E-VAF analysis for the nano viscous fluid problem in S-V.

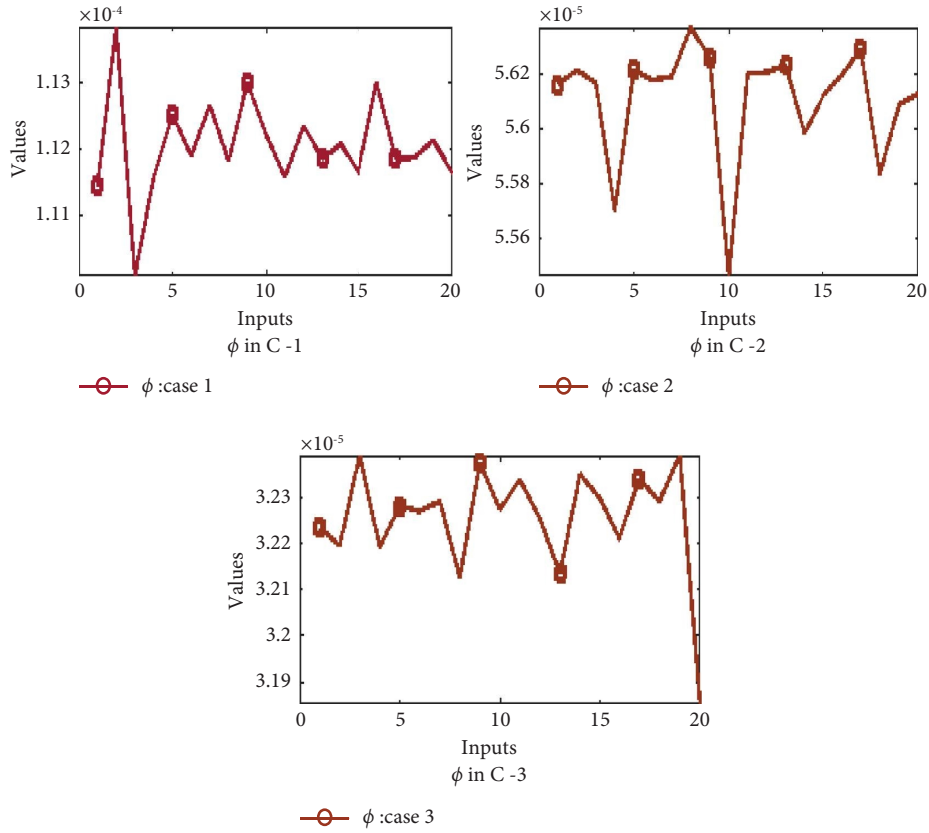

Figure 23: E-VAF analysis for the nano viscous fluid problem in S-VI.

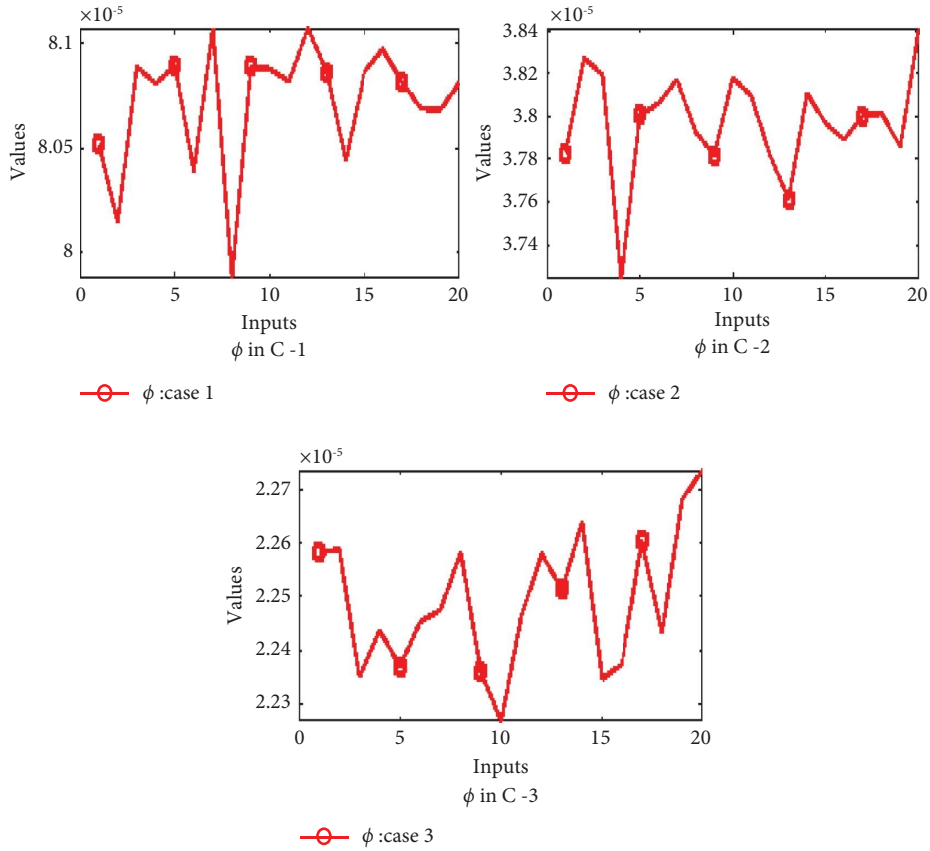

Figure 24: E-VAF analysis for the nano viscous fluid problem in S-VII.

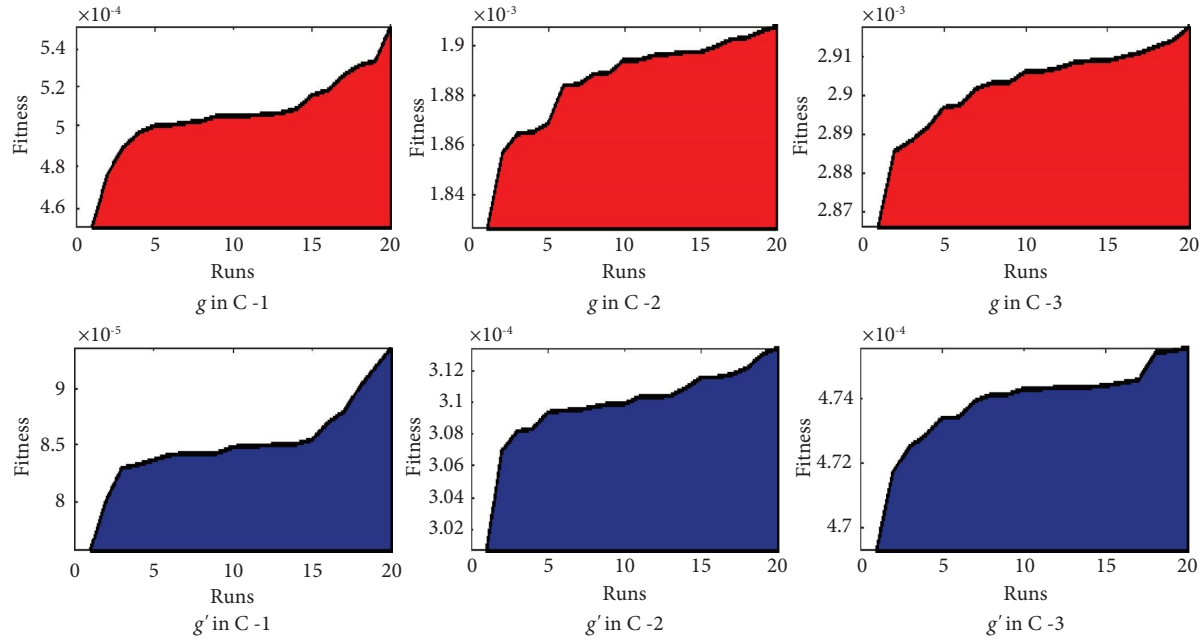

Figure 25: E-TIC based fitness analysis for the nano viscous fluid problem in S-I.

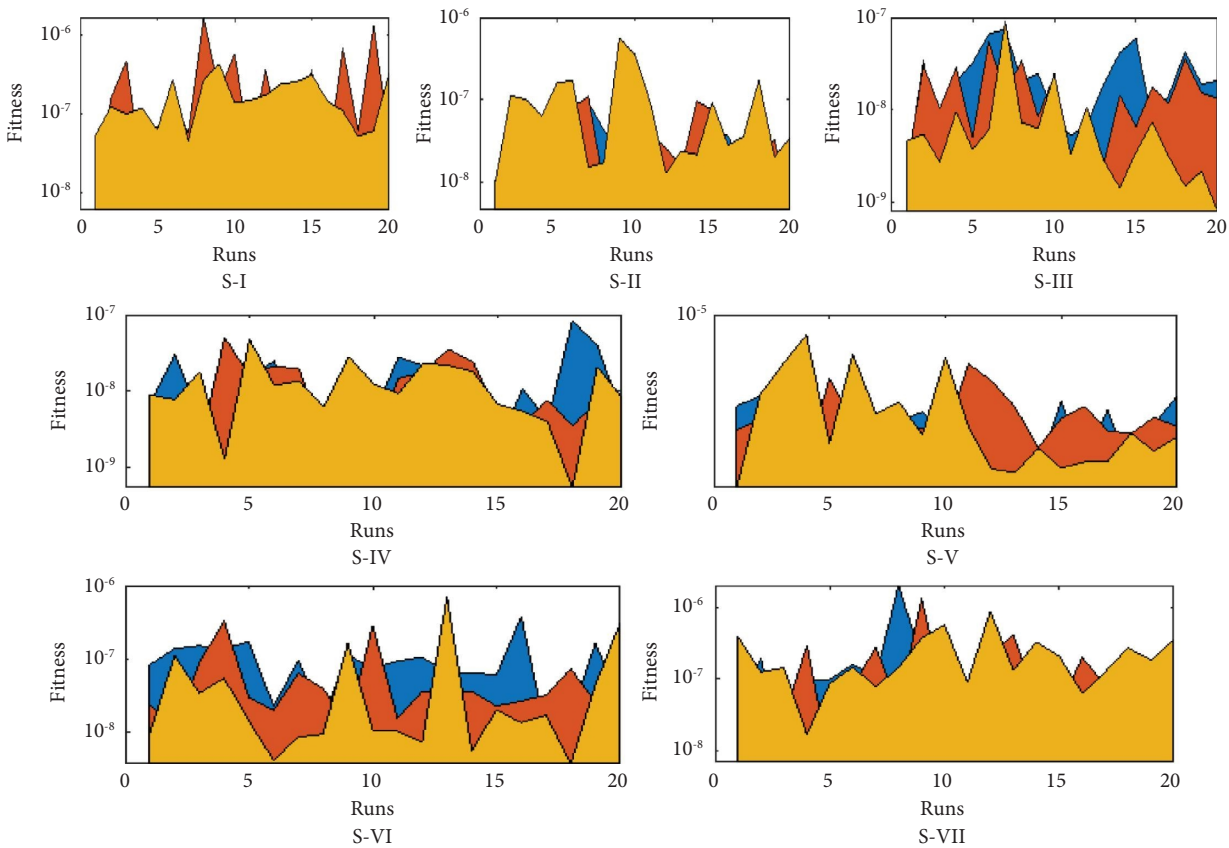

Figure 26: MAEs based fitness analysis for the nano viscous fluid problem in S (I–VII).

Table 3: Iteration with the best value in S (I–VII) of the suggested nanofluidic problem using the NHA-GA-SQP solver.

S-I						
	g					
Operator	C − 1		C − 2		C − 3	
	Best value (B. V)	It#	B. V	It#	B. V	It#
MAE	$3.776E-4$	10	$3.603E-4$	8	$3.709E-4$	11
RMSE	$4.623E-4$	10	$4.374E-4$	8	$4.466E-4$	11
E_TIC	$5.338E-4$	10	$5.051E-4$	8	$5.157E-4$	11
E_NSE	$1.453E-5$	10	$1.301E-5$	8	$1.356E-5$	11
E_VAF	$2.903E-7$	10	$2.511E-7$	8	$2.525E-7$	11
E_R^2	$1.453E-5$	10	$1.301E-5$	8	$1.356E-5$	11
	g'					
Operator	C − 1		C − 2		C − 3	
	B. V	It#	B. V	B. V	It#	B. V
MAE	$3.919E-4$	10	$3.622E-4$	8	$3.231E-4$	11
RMSE	$4.789E-4$	10	$4.380E-4$	8	$3.904E-4$	11
E_TIC	$5.530E-4$	10	$5.057E-4$	8	$4.508E-4$	11
E_NSE	$1.560E-5$	10	$1.304E-5$	8	$1.036E-5$	11
E_VAF	$3.091E-7$	10	$2.475E-7$	8	$1.959E-7$	5
E_R^2	$1.560E-5$	10	$1.304E-5$	8	$1.036E-5$	11
S-II						
	G					
Operator	C − 1		C − 2		C − 3	
	B. V	It#	B. V	B. V	It#	B. V
MAE	$3.571E-4$	15	$3.602E-4$	15	$1.495E-4$	9
RMSE	$4.330E-4$	15	$4.375E-4$	15	$1.674E-4$	9
E_TIC	$4.999E-4$	15	$5.052E-4$	15	$9.202E-5$	9
E_NSE	$1.275E-5$	15	$1.302E-5$	15	$1.821E-6$	9
E_VAF	$2.446E-7$	15	$2.516E-7$	15	$3.197E-8$	9
E_R^2	$1.275E-5$	15	$1.302E-5$	15	$1.821E-6$	9
	g'					
Operator	C − 1		C − 2		C − 3	
	B. V	It#	B. V	B. V	It#	B. V
MAE	$3.605E-4$	15	$3.614E-4$	15	$1.530E-4$	18
RMSE	$4.386E-4$	15	$4.374E-4$	15	$1.709E-4$	9
E_TIC	$5.065E-4$	15	$5.051E-4$	15	$9.393E-5$	9
E_NSE	$1.308E-5$	15	$1.301E-5$	15	$1.897E-6$	9
E_VAF	$2.547E-7$	11	$2.479E-7$	14	$3.265E-8$	9
E_R^2	$1.308E-5$	15	$1.301E-5$	15	$1.897E-6$	9
S-III						
	g					
Operator	C − 1		C − 2		C − 3	
	B. V	It#	B. V	B. V	It#	B. V
MAE	$1.331E-4$	6	$1.340E-4$	4	$1.298E-4$	16
RMSE	$1.544E-4$	6	$1.546E-4$	4	$1.531E-4$	16
E_TIC	$8.484E-5$	6	$8.497E-5$	4	$8.414E-5$	16
E_NSE	$1.547E-6$	6	$1.552E-6$	4	$1.522E-6$	16
E_VAF	$3.440E-8$	13	$3.346E-8$	4	$3.701E-8$	16
E_R^2	$1.547E-6$	6	$1.552E-6$	4	$1.522E-6$	16
	g'					
Operator	C − 1		C − 2		C − 3	
	B. V	It#	B. V	B. V	It#	B. V
MAE	$1.324E-4$	6	$1.175E-4$	4	$1.349E-4$	7
RMSE	$1.531E-4$	13	$1.384E-4$	4	$1.553E-4$	7
E_TIC	$8.414E-5$	13	$7.607E-5$	4	$8.537E-5$	7
E_NSE	$1.522E-6$	13	$1.244E-6$	4	$1.567E-6$	7
E_VAF	$3.317E-8$	15	$3.009E-8$	11	$3.335E-8$	16
E_R^2	$1.522E-6$	13	$1.244E-6$	4	$1.567E-6$	7
S-IV						

Table 3: Continued.

Operator	C − 1		C − 2		C − 3	
	B. V	It#	B. V	B. V	It#	B. V
			G			
MAE	$1.341E-4$	19	$1.303E-2$	4	$1.304E-2$	9
RMSE	$1.543E-4$	19	$1.518E-2$	4	$1.519E-2$	9
E_TIC	$8.481E-5$	19	$8.527E-3$	4	$8.532E-3$	9
E_NSE	$1.546E-6$	19	$1.438E-2$	4	$1.440E-2$	9
E_VAF	$3.266E-8$	19	$4.702E-4$	4	$4.706E-4$	9
E_R^2	$1.546E-6$	19	$1.438E-2$	4	$1.440E-2$	9
			g'			
Operator	C − 1		C − 2		C − 3	
	B. V	It#	B. V	B. V	It#	B. V
MAE	$1.326E-4$	19	$1.301E-2$	11	$1.302E-2$	5
RMSE	$1.531E-4$	19	$1.516E-2$	11	$1.517E-2$	9
E_TIC	$8.417E-5$	19	$8.515E-3$	11	$8.522E-3$	9
E_NSE	$1.523E-6$	19	$1.434E-2$	11	$1.436E-2$	9
E_VAF	$3.300E-8$	18	$4.696E-4$	4	$4.696E-4$	9
E_R^2	$1.523E-6$	19	$1.434E-2$	11	$1.436E-2$	9
			S-V			
			Θ			
Operator	C − 1		C − 2		C − 3	
	B. V	It#	B. V	B. V	It#	B. V
MAE	$1.304E-2$	4	$1.303E-2$	11	$1.303E-2$	4
RMSE	$1.518E-2$	4	$1.518E-2$	11	$1.517E-2$	4
E_TIC	$8.530E-3$	4	$8.527E-3$	11	$8.526E-3$	4
E_NSE	$1.439E-2$	4	$1.438E-2$	11	$1.438E-2$	4
E_VAF	$4.704E-4$	4	$4.704E-4$	11	$4.699E-4$	4
E_R^2	$1.439E-2$	4	$1.438E-2$	11	$1.438E-2$	4
			ϕ			
Operator	C − 1		C − 2		C − 3	
	B. V	It#	B. V	B. V	It#	B. V
MAE	$1.301E-2$	4	$1.298E-2$	16	$1.300E-2$	4
RMSE	$1.516E-2$	4	$1.513E-2$	16	$1.515E-2$	4
E_TIC	$8.517E-3$	4	$8.500E-3$	16	$8.510E-3$	4
E_NSE	$1.435E-2$	4	$1.429E-2$	16	$1.432E-2$	4
E_VAF	$4.696E-4$	4	$4.692E-4$	12	$4.695E-4$	4
E_R^2	$1.435E-2$	4	$1.429E-2$	16	$1.432E-2$	4
			S-VI			
			ϕ			
Operator	C − 1		C − 2		C − 3	
	B. V	It#	B. V	B. V	It#	B. V
MAE	$7.611E-3$	4	$7.602E-3$	12	$7.583E-3$	20
RMSE	$9.357E-3$	4	$9.353E-3$	12	$9.336E-3$	20
E_TIC	$5.358E-3$	4	$5.356E-3$	12	$5.346E-3$	20
E_NSE	$5.284E-3$	4	$5.281E-3$	12	$5.261E-3$	20
E_VAF	$3.171E-4$	3	$3.179E-4$	10	$3.176E-4$	20
E_R^2	$5.284E-3$	4	$5.281E-3$	12	$5.261E-3$	20
			S-VII			
			ϕ			
Operator	C − 1		C − 2		C − 3	
	B. V	It#	B. V	B. V	It#	B. V
MAE	$7.531E-3$	8	$7.564E-3$	9	$1.372E-3$	14
RMSE	$9.294E-3$	8	$9.325E-3$	9	$1.640E-3$	10
E_TIC	$5.322E-3$	8	$5.339E-3$	9	$1.894E-3$	10
E_NSE	$5.214E-3$	8	$5.248E-3$	9	$1.829E-4$	10
E_VAF	$3.177E-4$	8	$3.184E-4$	4	$3.297E-6$	10
E_R^2	$5.214E-3$	8	$5.248E-3$	9	$1.829E-4$	10

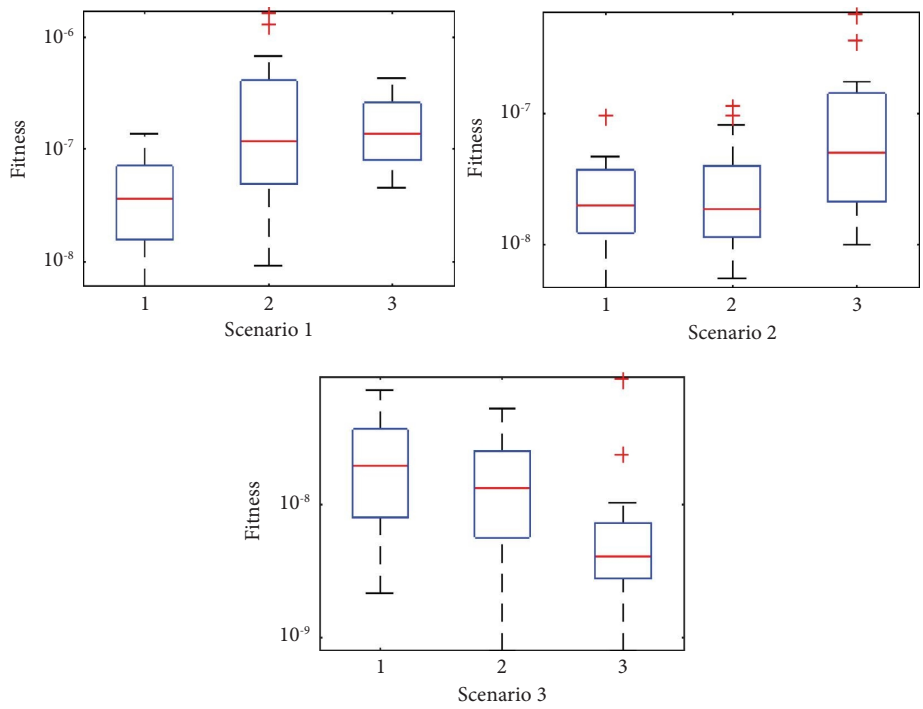

Figure 27: Fitness based on boxplot analysis for the nano viscous fluid problem in 1st three scenarios.

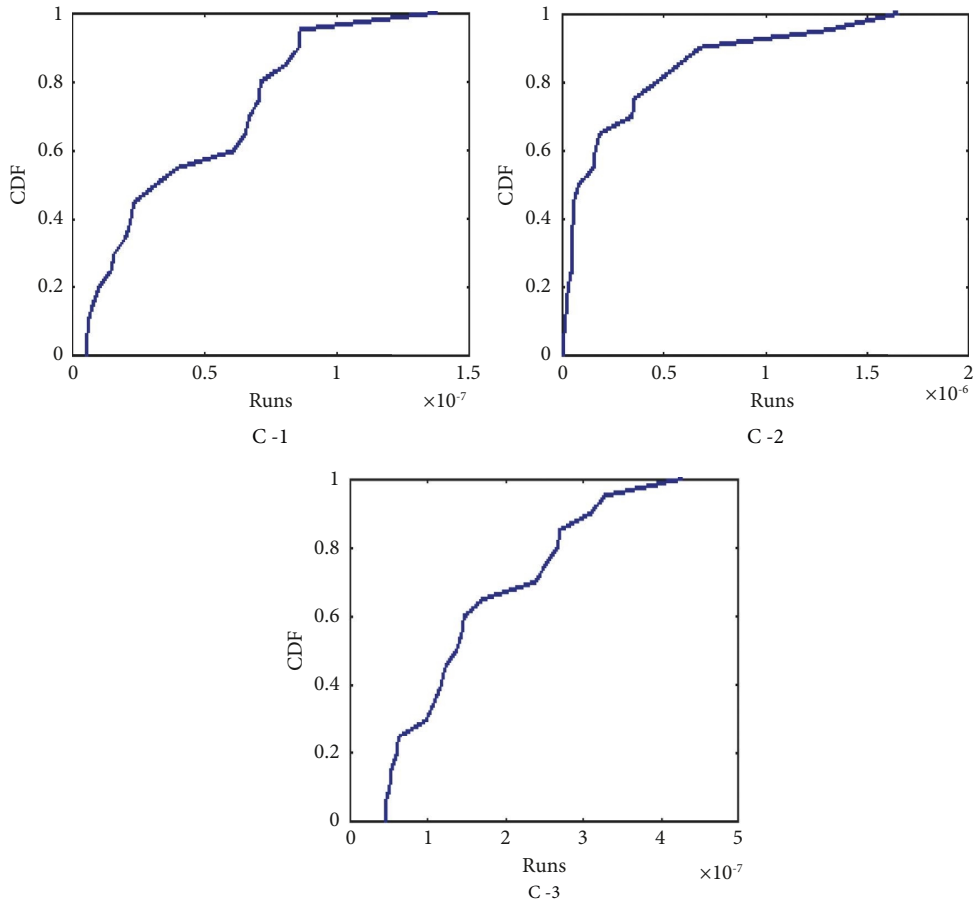

Figure 28: Fitness based on CDF analysis for the suggested nanofluidic problem in C (1–3) of S-I.

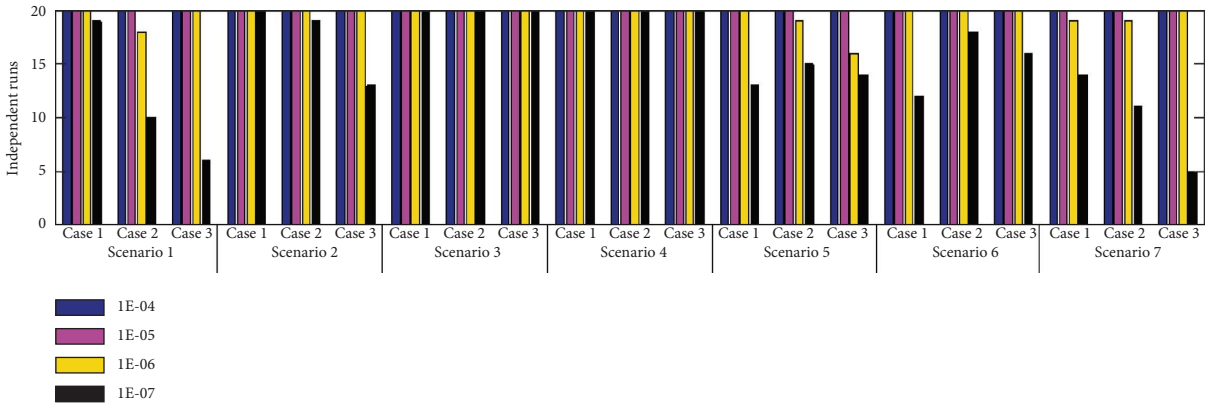

Figure 29: Convergence rate based on fitness estimation for the suggested nanofluidic problem S (I–VII).

5. Conclusion

The EMHD impacts on the nano viscous fluid model are investigated through the NHA-GA-SQP algorithm, and the most reliable approximate solution is successfully generated based on seven different scenarios by assigning distinct values to various physical parameters. Different statistical performance operators are used to analyze the speedy convergence, validity, and effectiveness of the suggested solver. The following are the highlights of the current research:

(i) A comparison with the reference solution shows that results generated through the designed algorithm are accurate up to 7 decimal places.

(ii) The higher convergence rate obtained through fitness estimation guarantees that the designed solver can easily attain the stiff criteria.

(iii) The analysis based on various statistical performance operators shows that the proposed method is quite reliable and robust for solving nonlinear systems of higher-order differential equations.

(iv) The velocity $\widehat{g}'(\eta)$ rises with the increase in the values of λ, E_1 and N_1 but shows a reversed impression in the case of M.

(v) The thermal profile $\widehat{\theta}(\eta)$ shows a rising trend for the growing values of N_b.

(vi) The concentration $\widehat{\phi}(\eta)$ diminishes against the rise in the values of S_c, N_b, and γ.

The NHA-GA-SQP emerge as a fine alternate to obtain results with high accuracy for the problems involving ODEs, PDEs, fuzzy, fractional, and functional equations having strong nonlinearity. In the future, this newly designed technique shall be a fine alternate to handle stiff nonlinear fluid problems.

Nomenclature

v_1, v_2: Velocity components
E_0: Strength of electric field
B_0: Strength of magnetic field
$v_{1w}(x)$: Sheet velocity
σ: Electrical conductivity
Q_0: Heat source/sink coefficient
$(\rho c_p)_g$: Heat capacity of base fluid
$(\rho c_p)_p$: Capacity of nanofluid
M: Magnetic parameter
λ: The mixed convection parameter
Br: Brinkman number
γ: Reaction parameter
S_c: Schmidt number
ρ_f: Density
Pr: Prandtl Number
D_T: Coefficient of thermophoresis diffusion
Tm_∞: Ambient temperature
C_∞: Concentration
D_B: Brownian diffusion coefficient
C: Nanofluid concentration
D_B: Brownian diffusion coefficient
E_1: Electric field parameter
Gr: Grashof number
N_1: Buoyancy ratio parameter
Nt: Thermophoresis parameter
β: Heat generation/absorption parameter
N_b: Brownian motion parameter
E_c: Eckert number.

Data Availability

The data used to support the findings of this study can be made available from the corresponding author upon request.

Conflicts of Interest

The authors declare that there are no conflicts of interest.

References

[1] H. Masuda, A. Ebata, and K. Teramae, "Alteration of thermal conductivity and viscosity of liquid by dispersing ultra-fine particles," *Dispersion of Al2O3, SiO2 and TiO2 Ultra-fine Particles*, Springer, Berlin, Germany, 1993.

[2] S. Akilu, K. V. Sharma, A. T. Baheta, and R. Mamat, "A review of thermophysical properties of water based composite

nanofluids," *Renewable and Sustainable Energy Reviews*, vol. 66, pp. 654–678, 2016.

[3] B. Bakthavatchalam, K. Habib, R. Saidur, B. B. Saha, and K. Irshad, "Comprehensive study on nanofluid and ionanofluid for heat transfer enhancement: a review on current and future perspective," *Journal of Molecular Liquids*, vol. 305, Article ID 112787, 2020.

[4] M. Sheikholeslami, B. Rezaeianjouybari, M. Darzi, A. Shafee, Z. Li, and T. K. Nguyen, "Application of nano-refrigerant for boiling heat transfer enhancement employing an experimental study," *International Journal of Heat and Mass Transfer*, vol. 141, pp. 974–980, 2019.

[5] S. U. Choi and J. A. Eastman, *Enhancing thermal Conductivity of Fluids with Nanoparticles (No. ANL/MSD/CP-84938; CONF-951135-29)*, Argonne National Lab, Argonne, IL, USA, 1995.

[6] K. N. Ramesh, T. K. Sharma, and G. Rao, "Latest advancements in heat transfer enhancement in the micro-channel heat sinks: a review," *Archives of Computational Methods in Engineering*, vol. 28, no. 4, pp. 3135–3165, 2021.

[7] D. H. Nguyen and H. S. Ahn, "A comprehensive review on micro/nanoscale surface modification techniques for heat transfer enhancement in heat exchanger," *International Journal of Heat and Mass Transfer*, vol. 178, Article ID 121601, 2021.

[8] S. Almurtaji, N. Ali, J. A. Teixeira, and A. Addali, "On the role of nanofluids in thermal-hydraulic performance of heat exchangers—a review," *Nanomaterials*, vol. 10, no. 4, p. 734, 2020.

[9] A. Kumar, M. A. Hassan, and P. Chand, "Heat transport in nanofluid coolant car radiator with louvered fins," *Powder Technology*, vol. 376, pp. 631–642, 2020.

[10] V. Salamon, D. Senthil kumar, and S. Thirumalini, "Experimental investigation of heat transfer characteristics of automobile radiator using tio2-nanofluid coolant IOP Conference Series: materials Science and Engineering," *IOP Conference Series: Materials Science and Engineering*, vol. 225, no. 1, Article ID 012101, 2017.

[11] M. A. Fikri, F. F. Asri, W. M. Faizal et al., "TiO_2-SiO_2 nanofluid characterization: towards efficient with water/ethylene glycol mixture for solar application," *IOP Conference Series: Materials Science and Engineering*, vol. 863, no. 1, Article ID 012055, 2020.

[12] S. Wiriyasart, C. Hommalee, S. Sirikasemsuk, R. Prurapark, and P. Naphon, "Thermal management system with nanofluids for electric vehicle battery cooling modules," *Case Studies in Thermal Engineering*, vol. 18, Article ID 100583, 2020.

[13] S. Nadeem, M. N. Khan, N. Muhammad, and S. Ahmad, "Mathematical analysis of bio- convective micropolar nanofluid," *Journal of Computational Design and Engineering*, vol. 6, no. 3, pp. 233–242, 2019.

[14] S. Ahmad and S. Nadeem, "Cattaneo–Christov-based study of SWCNT–MWCNT/EG Casson hybrid nanofluid flow past a lubricated surface with entropy generation," *Applied Nanoscience*, vol. 10, no. 12, pp. 5449–5458, 2020.

[15] S. Ahmad and S. Nadeem, "Flow analysis by Cattaneo–Christov heat flux in the presence of Thomson and Troian slip condition," *Applied Nanoscience*, vol. 10, no. 12, pp. 4673–4687, 2020.

[16] H. A. Alzahrani, A. Alsaiari, J. K. Madhukesh, R. Naveen Kumar, and B. M. Prasanna, "Effect of thermal radiation on heat transfer in plane wall jet flow of Casson nanofluid with suction subject to a slip boundary condition," *Waves in Random and Complex Media*, vol. 502, pp. 1–18, 2022.

[17] U. Khan, S. Ahmad, A. Hayyat, I. Khan, K. S. Nisar, and D. Baleanu, "On the Cattaneo–Christov heat flux model and OHAM analysis for three different types of nanofluids," *Applied Sciences*, vol. 10, no. 3, p. 886, 2020.

[18] S. Ahmad, S. Nadeem, N. Muhammad, and M. N. Khan, "Cattaneo–Christov heat flux model for stagnation point flow of micropolar nanofluid toward a nonlinear stretching surface with slip effects," *Journal of Thermal Analysis and Calorimetry*, vol. 143, no. 2, pp. 1187–1199, 2021.

[19] S. Ahmad, S. Nadeem, and N. Ullah, "Entropy generation and temperature-dependent viscosity in the study of SWCNT–MWCNT hybrid nanofluid," *Applied Nanoscience*, vol. 10, no. 12, pp. 5107–5119, 2020.

[20] M. G. Reddy, O. Tripathi, and B. Anwar, "Numerical modelling of electromagnetohydrodynamic (EMHD) radiative transport of hybrid Ti6Al4V-AA7075/H2O nanofluids from a riga plate sensor surface," in *Nanomaterials and Nanoliquids: Applications in Energy and Environment*, pp. 225–248, Springer Nature Singapore, Singapore, 2023.

[21] A. M. Obalalu, T. Oreyeni, A. Abbas et al., "Implication of electromagnetohydrodynamic and heat transfer analysis in nanomaterial flow over a stretched surface: applications in solar energy," *Case Studies in Thermal Engineering*, vol. 49, Article ID 103381, 2023.

[22] D. Saha, A. Mahanta, S. Mukhopadhyay, and S. Sengupta, "Cattaneo–Christov heat and mass flux model for Electromagnetohydrodynamic (EMHD) non-Newtonian flow of Jeffrey nanofluid with nonlinear thermal radiation and stratified boundary conditions," *Waves in Random and Complex Media*, vol. 718, pp. 1–25, 2023.

[23] R. Naz, M. Noor, T. Hayat, M. Javed, and A. Alsaedi, "Dynamism of magnetohydrodynamic cross nanofluid with particulars of entropy generation and gyrotactic motile microorganisms," *International Communications in Heat and Mass Transfer*, vol. 110, Article ID 104431, 2020.

[24] I. Tlili, H. A. Nabwey, M. G. Reddy, N. Sandeep, and M. Pasupula, "Effect of resistive heating on incessantly poignant thin needle in magnetohydrodynamic Sakiadis hybrid nanofluid," *Ain Shams Engineering Journal*, vol. 12, no. 1, pp. 1025–1032, 2021.

[25] K. Al-Farhany, K. K. Al-Chlaihawi, M. F. Al-dawody, N. Biswas, and A. J. Chamkha, "Effects of fins on magnetohydrodynamic conjugate natural convection in a nanofluid-saturated porous inclined enclosure," *International Communications in Heat and Mass Transfer*, vol. 126, Article ID 105413, 2021.

[26] S. Zaman and M. Gul, "Magnetohydrodynamic bioconvective flow of Williamson nanofluid containing gyrotactic microorganisms subjected to thermal radiation and Newtonian conditions," *Journal of Theoretical Biology*, vol. 479, pp. 22–28, 2019.

[27] A. Ayub, H. A. Wahab, Z. Sabir, and A. Arbi, "A note on heat transport with aspect of magnetic dipole and higher order chemical process for steady micropolar fluid," *Computational overview of fluid structure interaction*, vol. 97, 2020.

[28] I. Ahmad, S. I. Hussain, M. A. Z. Raja, and M. Shoaib, "Transportation of hybrid MoS_2-SiO_2/EG nanofluidic system toward radially stretched surface," *Arabian Journal for Science and Engineering*, vol. 48, no. 1, pp. 953–966, 2023.

[29] I. Ahmad, H. Ilyas, K. Kutlu, V. Anam, S. I. Hussain, and J. L. G. Guirao, "Numerical computing approach for solving

Hunter-Saxton equation arising in liquid crystal model through sinc collocation method," *Heliyon*, vol. 7, no. 7, Article ID e07600, 2021.

[30] I. Ahmad, S. I. Hussain, M. Usman, and H. Ilyas, "On the solution of Zabolotskaya–Khokhlov and Diffusion of Oxygen equations using a sinc collocation method," *Partial Differential Equations in Applied Mathematics*, vol. 4, Article ID 100066, 2021.

[31] S. I. Hussain, I. Ahmad, M. A. Z. Raja, and C. M. Z. Umer, "A computational convection analysis of SiO2/water and MoS2-SiO2/water based fluidic system in inverted cone," *Engineering Reports*, vol. 5, no. 11, Article ID e12660, 2023.

[32] I. Ahmad, S. U. I. Ahmad, K. Kutlu, H. Ilyas, S. I. Hussain, and F. Rasool, "On the dynamical behavior of nonlinear Fitzhugh–Nagumo and Bateman–Burger equations in quantum model using Sinc collocation scheme," *The European Physical Journal Plus*, vol. 136, no. 11, p. 1108, 2021.

[33] S. Kwon, "Optimal feature selection based speech emotion recognition using two-stream deep convolutional neural network," *International Journal of Intelligent Systems*, vol. 36, no. 9, pp. 5116–5135, 2021.

[34] S. Lu, Z. Zhu, J. M. Gorriz, S. H. Wang, and Y. D. Zhang, "NAGNN: classification of COVID-19 based on neighboring aware representation from deep graph neural network," *International Journal of Intelligent Systems*, vol. 37, no. 2, pp. 1572–1598, 2022.

[35] A. K. Bhullar, R. Kaur, and S. Sondhi, "Modified neural network algorithm based robust design of AVR system using the Kharitonov theorem," *International Journal of Intelligent Systems*, vol. 37, no. 2, pp. 1339–1370, 2022.

[36] H. Wang, H. Zhang, J. Hu, Y. Song, S. Bai, and Z. Yi, "DeepEC: an error correction framework for dose prediction and organ segmentation using deep neural networks," *International Journal of Intelligent Systems*, vol. 35, no. 12, pp. 1987–2008, 2020.

[37] G. Agarwal, H. Om, and S. Gupta, "A learning framework of modified deep recurrent neural network for classification and recognition of voice mood," *International Journal of Adaptive Control and Signal Processing*, vol. 36, no. 8, pp. 1835–1859, 2022.

[38] W. Liu and M. Chen, "An adaptive anti-swing control for the helicopter slung-load system based on trajectory planning and neural network," *International Journal of Adaptive Control and Signal Processing*, vol. 36, no. 5, pp. 1116–1140, 2022.

[39] M. Piao, P. Tan, Y. Wang, M. Sun, B. Lu, and Z. Chen, "Disturbance observer-based robust motor control enhanced by adaptive neural network in the absence of velocity measurement," *International Journal of Robust and Nonlinear Control*, vol. 32, no. 9, pp. 5023–5047, 2022.

[40] L. Guo, T. Wang, Z. Wu et al., "Portable food-freshness prediction platform based on colorimetric barcode combinatorics and deep convolutional neural networks," *Advanced Materials*, vol. 32, no. 45, Article ID 2004805, 2020.

[41] R. Jafari, P. Spincemaille, J. Zhang et al., "Deep neural network for water/fat separation: supervised training, unsupervised training, and no training," *Magnetic Resonance in Medicine*, vol. 85, no. 4, pp. 2263–2277, 2021.

[42] C. Willers, G. Bauman, S. Andermatt et al., "The impact of segmentation on whole-lung functional MRI quantification: repeatability and reproducibility from multiple human observers and an artificial neural network," *Magnetic Resonance in Medicine*, vol. 85, no. 2, pp. 1079–1092, 2021.

[43] L. Chen, G. Canton, W. Liu et al., "Fully automated and robust analysis technique for popliteal artery vessel wall evaluation (FRAPPE) using neural network models from standardized knee MRI," *Magnetic Resonance in Medicine*, vol. 84, no. 4, pp. 2147–2160, 2020.

[44] A. J. Daniel, C. E. Buchanan, T. Allcock et al., "Automated renal segmentation in healthy and chronic kidney disease subjects using a convolutional neural network," *Magnetic Resonance in Medicine*, vol. 86, no. 2, pp. 1125–1136, 2021.

[45] I. Ahmad, M. A. Z. Raja, H. Ramos, M. Bilal, and M. Shoaib, "Integrated neuro-evolution-based computing solver for dynamics of nonlinear corneal shape model numerically," *Neural Computing and Applications*, vol. 33, no. 11, pp. 5753–5769, 2021.

[46] I. Ahmad, S. I. Hussain, H. Ilyas et al., "Numerical solutions of Schrödinger wave equation and Transport equation through Sinc collocation method," *Nonlinear Dynamics*, vol. 105, no. 1, pp. 691–705, 2021.

[47] F. Shahid, A. Zameer, A. Mehmood, and M. A. Z. Raja, "A novel wavenets long short term memory paradigm for wind power prediction," *Applied Energy*, vol. 269, Article ID 115098, 2020.

[48] I. Ahmad, S. I. Hussain, H. Ilyas, S. Jabeen, and A. Iqrar, "On the applications of collocation method for numerically analyzing the nonlinear Degasperis–Procesi and Benjamin–Bona–Mahony equations," *International Journal of Modern Physics B*, Article ID 2450264, 2023.

[49] I. Ahmad, S. U. I. Ahmad, F. Ahmad, and M. Bilal, "Neuro-Heuristic Computational Intelligence for nonlinear Thomas-Fermi equation using trigonometric and hyperbolic approximation," *Measurement*, vol. 156, Article ID 107549, 2020.

[50] Z. Sabir, S. Saoud, M. A. Z. Raja, H. A. Wahab, and A. Arbi, "Heuristic computing technique for numerical solutions of nonlinear fourth order Emden–Fowler equation," *Mathematics and Computers in Simulation*, vol. 178, pp. 534–548, 2020.

[51] Z. Sabir, M. A. Z. Raja, A. Arbi, G. C. Altamirano, and J. Cao, "Neuro-swarms intelligent computing using Gudermannian kernel for solving a class of second order Lane-Emden singular nonlinear model," *AIMS Mathematics*, vol. 6, no. 3, pp. 2468–2485, 2020.

[52] Z. Sabir, M. A. Z. Raja, S. E. Alhazmi, M. Gupta, A. Arbi, and I. A. Baba, "Applications of artificial neural network to solve the nonlinear COVID-19 mathematical model based on the dynamics of SIQ," *Journal of Taibah University for Science*, vol. 16, no. 1, pp. 874–884, 2022.

[53] D. Whitley, "A genetic algorithm tutorial," *Statistics and Computing*, vol. 4, no. 2, pp. 65–85, 1994.

[54] Q. Luo, Y. Rao, and D. Peng, "GA and GWO algorithm for the special bin packing problem encountered in field of aircraft arrangement," *Applied Soft Computing*, vol. 114, Article ID 108060, 2022.

[55] I. Ahmad, H. Ilyas, S. I. Hussain, and M. A. Z. Raja, "Evolutionary techniques for the solution of bio-heat equation arising in human dermal region model," *Arabian Journal for Science and Engineering*, vol. 5, pp. 1–26, 2023.

[56] R. Samadi and J. Seitz, "EEC-GA: energy-efficient clustering approach using genetic algorithm for heterogeneous wireless sensor networks," in *Proceedings of the 2022 International Conference on Information Networking (ICOIN)*, pp. 280–286, IEEE, Jeju-si, Korea, January 2022.

[57] J. Zhang, X. Qiu, X. Li, Z. Huang, M. Wu, and Y. Dong, "Corrigendum to "support vector machine weather prediction technology based on the improved quantum optimization algorithm," *Computational Intelligence and Neuroscience*, vol. 2022, Article ID 9762403, 2022.

[58] E. Yildirm and B. Denizhan, "A two-echelon pharmaceutical supply chain optimization via genetic algorithm," in *Recent Advances in Intelligent Manufacturing and Service Systems*, pp. 77–87, Springer, Singapore, 2022.

[59] I. Ahmad, S. I. Hussain, H. Ilyas, L. Zoubir, M. Javed, and M. A. Zahoor Raja, "Integrated stochastic investigation of singularly perturbed delay differential equations for the neuronal variability model," *International Journal of Intelligent Systems*, vol. 2023, Article ID 1918409, 24 pages, 2023.

[60] J. Li, E. Kebreab, F. You et al., "The application of nonlinear programming on ration formulation for dairy cattle," *Journal of Dairy Science*, vol. 105, no. 3, pp. 2180–2189, 2022.

[61] Y. Zhang, Y. Liu, Y. Huang et al., "An optimal control strategy design for plug-in hybrid electric vehicles based on internet of vehicles," *Energy*, vol. 228, Article ID 120631, 2021.

[62] M. Fawad Khan, E. Bonyah, F. S. Alshammari, S. M. Ghufran, and M. Sulaiman, "Modelling and analysis of virotherapy of cancer using an efficient hybrid soft computing procedure," *Complexity*, vol. 2022, Article ID 9660746, 29 pages, 2022.